IN SITU U-PB GEOCHRONOLOGY OF PEROVSKITE AND SCHORLOMITE GARNET FROM MAGNET COVE, AR: NEW AGE CONSTRAINTS ON ALKALINE MAGMATISM AND SUITABILITY AS REFERENCE MATERIALS

By

Dalton Pell
B.S. University of Kansas 2023

Submitted to the graduate degree program in Geology and the Graduate Faculty of the University of Kansas in partial fulfillment of the requirements for the degree of Bachelor of Science.

_____

Chair: Rick Devlin

_____

Co-supervisor: Andreas Möller

_____

Co supervisor: Alison Olcott

_____

Co-supervisor: Noah McLean

Date Approved: May 2023

Abstract

The Magnet Cove Igneous Complex (MCIC) in Arkansas consists of multiple ring dikes of silica undersaturated rocks including various syenites, ijolites, phonolites, trachytes, and carbonatite (Erickson and Blade, 1963). The emplacement of the rocks is hypothesized to be from outside-in, with the outermost syenite ring emplaced first, and the carbonatite last (Erickson and Blade, 1963). There is an abundance of titanium- and zirconium-rich minerals including perovskite, titanite, and schorlomite, kimzeyite garnet. This study used laser ablation inductively coupled plasma mass spectrometry (LA-ICP-MS) after petrography characterization to date emplacement of the MCIC and test if these Ti minerals are suitable as U-Pb reference materials. Results will contribute to the discussion on the cause of Cretaceous magmatism in the midcontinent US.

One perovskite grain was analyzed with 34 spots of 35μ size. Of the garnets, multiple grains were analyzed and the number was dependent on rock type, surface area of the grain, and inclusion-rich material. Upwards of 40 spots were used on each rock type and were all 85μm. 85μm size was based on U and Pb concentrations.

The age of perovskite was initially calculated to be **85.7 ± 5.5** Ma, which is slightly younger than previous estimates of the MCIC. However, when the common Pb ratio was anchored at 0.82 ± 0.04, it is closer to other calculated ages at **100.5 ± 1.7 Ma**. Garnet ages were calculated from four different rock types: fine-grained ijolite (FGI), garnet-pseudoleucite syenite (GPS), garnet ijolite (GI), and garnet-biotite ijolite (GBI). Each rock achieved a slightly different age; however, the age range sits within the bounds between 98.1 Ma and102.8 Ma, which is consistent with the estimates for the magmatism in the Arkansas Alkaline Province (AAP). FGI: **98.5 ± 0.6 Ma**, GPS: **101.4 ± 0.5** or **101.1 ± 0.5** with an anchored common Pb at 0.8 ± 0.08, GI:

98.1 ± 0.6 Ma, GBI: **102.8 ± 0.6 Ma**. U-Pb dating of schorlomite by LA-ICP-MS is ongoing and will test their use as potential reference materials in future studies.

Keywords: Magnet Cove Igneous Complex, ring dike, continental magmatism, laser ablation inductively coupled plasma mass spectrometry, geochronology, reference materials, uranium lead dating

Acknowledgments

I would like to grant my extraordinary appreciation to Dr. Andreas Möller, my advisor on this project, as well as an integral part of my success at the University of Kansas. He provided me the opportunity to take my Undergraduate career to the next level and participate in a complex and brand-new research project. Despite numerous time conflicts due to our tortuous schedules, he understood and was always willing to make the best of it. I will always remember that unconditional support throughout the entire process. I would also like to thank Dr. Alison Olcott, Dr. Rick Devlin, and Dr. Noah McLean, three professors who provided me with advice and understanding for the production of this thesis. I appreciate their feedback and willingness to be members of the committee. I would like to thank Dr. Diane Kamola, who has been an immense supporter of me during my time at KU. My partner, Jessica Brown, ended up being collateral damage from this entire process. She heard my thoughts, my rants, and constant status updates. Her willingness to listen and her constant encouragement kept me afloat, and for that I give her the warmest thank you. My gratitude goes to my friends and family members, who not only supported this project, but all my endeavors, past and future. Finally, I would like to dedicate this paper to my grandmother, Carmen Sonia Soto-Bair, who unfortunately passed away in February of last year. She was a beacon of knowledge for the entire family, and always reinforced the importance of education. I know she would be tremendously proud of where I am today.

Table of Contents

Chapter 1: Introduction 1

Chapter 2: Geologic Setting 6

Previous Work 2.1 6

Geologic History 2.2 6

Previous Radiometric Data 2.3 8

Chapter 3: Methods 10

Sample Materials 3.1 10

Sample Methods 3.2 11

Sample Petrography and Preparation 11

LA-ICP-MS U-Pb Methodology 20

Laser Ablation Reference Material Data 22

Chapter 4: Results 26

LA-ICP-MS U-Pb Results 25

MCIC carbonatite perovskite (MCper) 26

MCIC Garnet-Pseudoleucite Syenite (MC-7) 30

MCIC Garnet Ijolite (MC-11) 33

MCIC Garnet-Biotite Ijolite (MC-30) 35

Chapter 5: Discussion 37

Chapter 6: Conclusions and Future Work 42

References 45

Appendix A: U-Pb Perovskite Data 52

Appendix B: U-Pb Ti-Garnet Data Session 56

Appendix C: Additional Maps of the Magnet Cove Igneous Complex..... 62

List of Figures

Figure 1. Simplified geologic map of the Magnet Cove Igneous Complex, AR 5

Figure 2. Stratigraphic table showing the sedimentary units of Magnet Cove, AR 7

Figure 3. Geologic map of the greater Magnet Cove area and the nearby structure 8

Figure 4. Perovskite from the MCIC carbonatite mounted in epoxy 11

Figure 5. Plain and crossed polarized light images of sample MC-5 12

Figure 6. Hand sample image of sample MC-5 13

Figure 7. Plain and crossed polarized light images of sample MC-7 14

Figure 8. Hand sample image of sample MC-7 15

Figure 9. Plain and crossed polarized light images of sample MC-11 16

Figure 10. Hand sample image of sample MC-11 17

Figure 11. Plain and crossed polarized light images of sample MC-30 18

Figure 12. TW-Concordia diagram for MCper age calibration reference material IR6. 22

Figure 13. TW-Concordia diagram for MCper age validation reference material Afr/EAfr 23

Figure 14. TW-Concordia diagram for garnet age calibration reference material Mali 24

Figure 15. TW-Concordia diagram for garnet age validation reference material LJ 24

Figure 16. Reflected light image of spot traverses on MCper 26

Figure 17. TW-Concordia diagram plot for U-Pb dating of Sample MCper 27

Figure 18. Reflected light image of spot traverses on MC-5 28

Figure 19. TW-Concordia diagram for U-Pb dating of sample MC-5 29

Figure 20. Reflected light image of spot traverses on MC-7 30

Figure 21. Transmitted light image of spot traverses across garnet zoning on MC-7 31

Figure 22. TW-Concordia diagram for U-Pb dating of sample MC-7 32

Figure 23. Reflected light image of spot traverses on MC-11 33

Figure 24. TW-Concordia diagram for U-Pb dating of sample MC-11..... 34

Figure 25. Reflected light image of spot traverses on MC-30 35

Figure 26. Transmitted light image of spot traverses across garnet zoning on MC-30 36

Figure 27. TW-Concordia diagram for U-Pb dating of sample MC-30..... 37

Figure 28. Tectono-magmatic sequence for AR, KS midcontinent magmatism 41

Figure 29. Plot showing $^{87}Sr/^{86}Sr$ and εNd vs. time within the Arkansas Alkalic Province..... 42

List of Tables

Table 1. Data Reporting Table for Perovskite Analysis..... 20

Table 2. Data Reporting Table for Garnet Analysis..... 22

Table 3. LA-ICP-MS U-Th-Pb Data for reference material IR6 52

Table 4. LA-ICP-MS U-Th-Pb Data for reference material Afr..... 53

Table 5. LA-ICP-MS U-Th-Pb Data for sample EAfr 54

Table 6. LA-ICP-MS U-Th-Pb Data for sample MCper..... 55

Table 7. LA-ICP-MS U-Th-Pb Data for reference material Mali..... 56

Table 8. LA-ICP-MS U-Th-Pb Data for sample MC-LJ 57

Table 9. LA-ICP-MS U-Th-Pb Data for sample MC-5 58

Table 10. LA-ICP-MS U-Th-Pb Data for sample MC-7 59

Table 11. LA-ICP-MS U-Th-Pb Data for sample MC-11 60

Table 12. LA-ICP-MS U-Th-Pb Data for sample MC-30 61

Chapter 1: Introduction

Magnet Cove is a ring dike igneous complex in central Arkansas (Fig. 1). The rocks contain a variety of minerals, some first described from the MCIC (e.g., kimzeyite garnet; Milton et al. 1961), of interest to rare mineral collectors, and potentially of interest for the exploration and recovery of critical minerals (e.g. Howard et al. 2007) with Rare Earth Elements (REE) present like Niobium, Lithium, and Vanadium (Flohr, 1994). Titanium minerals are sometimes primary constituents of the rocks of MCIC. These minerals include perovskite, garnets of varying Ti enrichment, and titanite (sphene). Schorlomite is the garnet of focus for this study and is a Ti-rich garnet with formula $Ca_3Ti_2(SiO_4)(Fe^{3+}O_4)_2$ where wt% of TiO_2 exceeds 15% (Flohr and Ross, 1989). Uranium can replace the Ti within the crystal structure, rendering the minerals datable via the U-Pb radiometric method.

Utilizing the U-Pb decay method has the potential for more robust ages than previously used techniques because of its high closure temperatures and resistance to alteration. Perovskite has been dated by LA-ICP-MS before and can be used as reference material from some localities (e.g. Reguir 2010, Simonetti and Tappe, 2012). Interest in perovskite geochronology comes from its ability to date rocks that may lack zircon (Heaman, 2004) and therefore can provide ages for silica undersaturated rocks like lamproites and kimberlites. This study also dates garnets of various Ti enrichment. Garnet minerals can form in metamorphic and skarn deposits, making their use as a geochronometer important for determining ages of metamorphism and metasomatism (Burisch et al., 2019; Chen et al., 2022; Millonig et al., 2008). Previous radiometric studies used K-Ar and Rb-Sr dating of biotite (Zartman et al., 1967) and whole rock (Baldwin and Adams, 1971), Ar-Ar dating of biotite (Baksi, 1997) and fission-track dating of apatite and titanite (Arne, 1992; Eby and Vasconcelos, 2009; Sharon and Hsu 1969) and

established a Mid to Late-Cretaceous intrusive history. Further details are given in the Geologic Setting Chapter. However, it has to be noted that all these methods have only moderately high closure temperatures of ranges between 600°C and 700°C for titanite (Scott and St-Onge, 1995; Pidgeon et al., 1996) and 375°C to 600°C for apatite (Kirkland et al., 2018), compared to 800°C for garnet (Jung and Metzger, 2003). By calculating more and robust ages than previous studies, there is potential to determine more exact relative ages between the different units by dating their crystallization and emplacement. The rock types that have been dated from the MCIC are carbonatite, ijolite, jacupirangite, phonolite, trachyte, and various syenites. The youngest age obtained was from fission tracks in apatite from the carbonatite at 90 ± 9 Ma (Sharon and Hsu, 1969). The oldest was a titanite fission track age from an undifferentiated syenite at 105 ± 10 Ma (Sharon and Hsu, 1969). However, most studies have obtained ages between 95 Ma and 98 Ma, (Arne, 1992; Baksi, 1997; Baldwin and Adams, 1971; Eby and Vasconcelos, 2009; Zartman et al., 1967). Almost all dates overlap with each other when incorporating statistical uncertainties. The current calculated uncertainties are thus too high to determine a precise order of emplacement, i.e., within uncertainty limits, the carbonatite (90 ± 9 Ma; Sharon & Hsu, 1969) could have been emplaced before the pseudoleucite syenite, dated from titanite (96.9 ± 22.3 Ma; Eby and Vasconcelos, 2009), which does not agree with the outside-in emplacement model from Erickson and Blade (1963).

Therefore, establishing a more precise age for the rock units of the Magnet Cove igneous complex is necessary to compare them more effectively to other magmatic activity within the United States, such as the occurrence of lamproites and kimberlites in Kansas (Brookins, 1970; Brookins and Naeser, 1971). This could facilitate the further evaluation of different models that

may provide a greater level of insight into the driving force of midcontinent magmatism during the Mid-Cretaceous.

The current models proposed include hot spot magmatism, crustal extension, and subduction of fragments of the Farallon plate. The hot spot theory traces the igneous activity to the Bermuda hot spot, which some studies model to pass directly through or near the Arkansas alkaline province (AAP) (Duncan, 1984, Morgan, 1983). However, this theory has been questioned due to other Cretaceous igneous activity within the United States that conflicts with the Bermuda hot spot forming an age progressive trace through Arkansas and Kansas (Vogt and Jung, 2007). The crustal extension theory relies on the fact that the AAP is situated on the flank of the Mississippi graben and occurs in a zone of weak crust and transform faults (Thomas, 2006). Additionally, there is a boundary between low- and high-density mantle just South of the AAP (Eby and Vasconcelos, 2009). The proposed uplift from Cox and Van Arsdale (1997, 2002) is hypothesized to occur at the same time as the AAP, which would in turn be the cause for the extension and therefore crustal failure, leading to mantle upwelling and decompression melting, forming the AAP (Eby and Vasconcelos, 2009). This theory can be further supported by εNd values and $^{87}Sr/^{86}Sr$ ratios indicating an early lithospheric source followed by more asthenosphere dominated, which shows melt progression, and the source of melt became deeper over time (Duke et al., 2014). However, the isotopic compositions can also support an oceanic lithosphere subduction theory due to the similarities and trends of εNd values and $^{87}Sr/^{86}Sr$ ratios from igneous alkaline provinces that trend nearly linear N40^{o}W between Louisiana and Alberta (Duke et al., 2014).

Reference materials are required for calibration when conducting laser ablation – inductively coupled – mass spectrometry (LA-ICP-MS) analyses due to the need for correction

of laser-induced element and isotope fractionation and machine drift (e.g., Paton et al. 2011). Currently, there are few perovskite and schorlomite (garnet) reference materials readily available (e.g. Seman et al. 2017; Reguir et al. 2021; Aysal et al. 2023 in press). Research for identifying localities with garnets of reference material quality is ongoing (e.g., Aysal et al., 2023). Good reference materials need to be readily available and easily extracted, yield precise ages, repeatable on multiple grains, and have age homogeneity within grains. Since most perovskites and garnet do not yield concordant results but rely on isochrons with a well-defined lower concordia intercept, internal zoning in Pb/Pb vs U/Pb isotope space (Tera-Wasserburg concordia diagram, TW) is an advantage. In addition to calculating mineral ages, this study aims at testing the suitability of perovskite and schorlomite from the MCIC as potential reference materials.

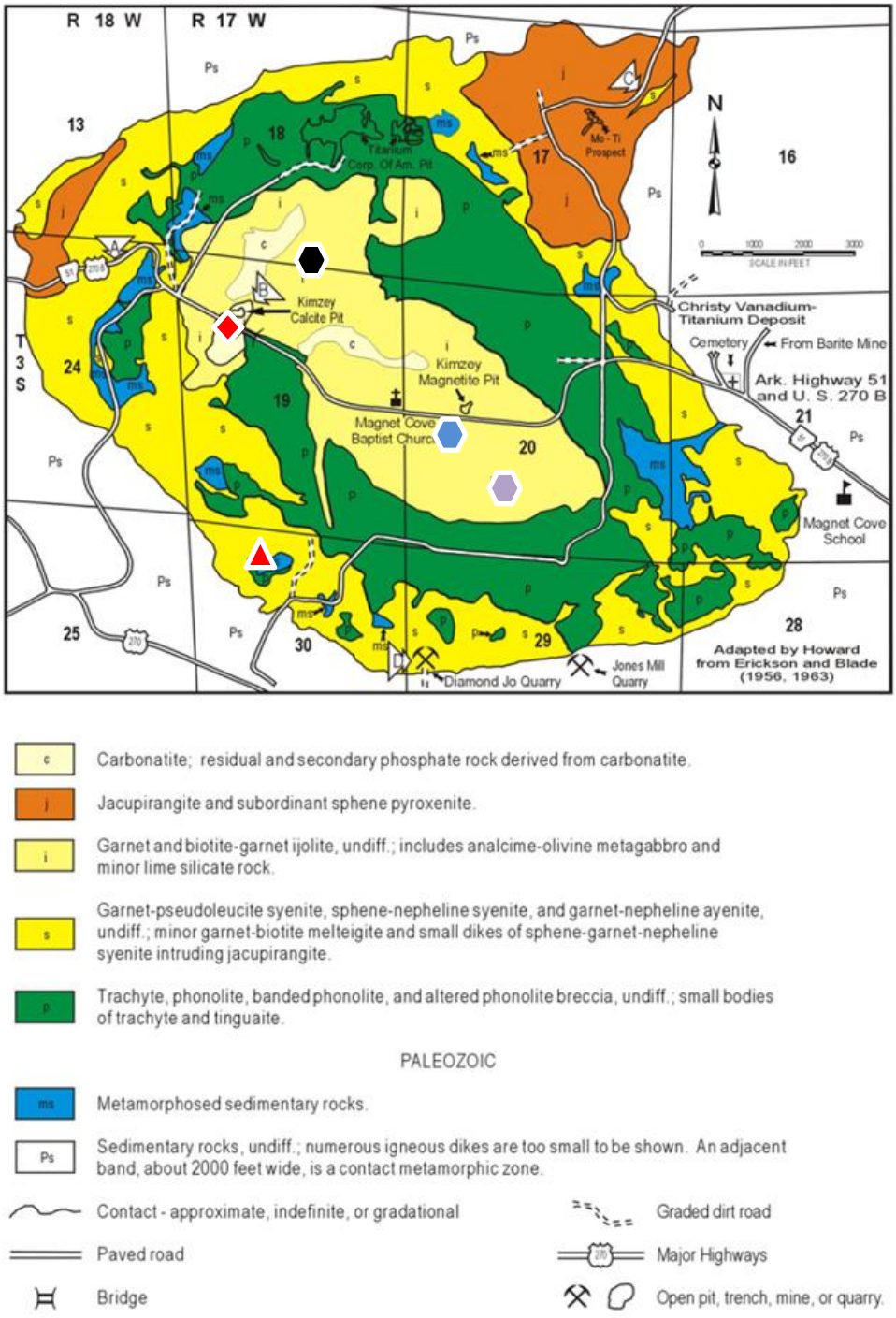

Figure 1: Simplified geologic map of the Magnet Cove Igneous Complex only show the major rock types. The map was adapted from the original published by Erickson and Blade (1963), simplified by Flohr and Ross (1989), and colored by the Arkansas Geological Survey, and adapted by Howard (2007). Samples labels of this study were placed in their hypothesized location based on rock type. Shapes are grouped based on similar rock types. Red triangle: MCper; Black hexagon: MC-5, Red diamond: MC-7; Periwinkle hexagon: MC-11; Blue hexagon: MC-30. Detailed contacts of non-generalized rock types can be seen on the Erickson & Blade (1963) map in Appendix C.

Chapter 2: Geologic Setting

This chapter first describes historic mapping, the geologic structure and history of the of the MCIC, and then the previous geochronologic studies.

Previous Work 2.1

The Magnet Cove igneous complex (MCIC) has been mapped and studied extensively multiple times over the course of about seventy years (Erickson and Blade, 1963). The MCIC was first mapped in 1891 by Williams. The studies leading up to this map's publication included many mineralogical studies from the Magnet Cove area, starting in 1806 by Macrery. Washington reexamined Williams' map and published a new version in 1900, immediately followed by chemical analyses and revised rock names and descriptions in 1901. The mineralogical aspect of the MCIC was thoroughly studied and published in 1931 by Landes, which listed the known minerals within each rock type of the complex and mapped the ring dike structure by rock type. The most complete study of the entire MCIC remains the professional paper by Erickson and Blade (1963). However, multiple geochemical and mineralogical analyses have been performed since then to explore the rare minerals and rock types that the MCIC hosts (Flohr and Ross, 1990; Baksi, 1997; Eby and Vasconcelos, 2009; Metzger et al. 1977; Nesbitt and Kelly, 1977).

Geologic History 2.2

The MCIC as referenced in this study is located in Hot Spring County, AR, just Southwest of Little Rock. The area consists of Mid to Late Cretaceous igneous alkaline intrusive rocks. Much of the area is covered in vegetation, and most of the easily accessible rock is float. The complex consists of concentric ring dikes of intruding syenites, phonolites, jacupirangites, ijolites, carbonatites, and the overlying Paleozoic sediments (Fig. 2) (Erickson and Blade, 1963).

Each rock type can be further subdivided depending on whether specific minerals are present (eg. garnet ijolite and garnet-biotite ijolite). The carbonatite and ijolite occupy the low-lying core of the complex, and the syenites represent the ridges, with two intrusions of jacupirangite at the very Northeast and Northwest edges being the exceptions (Fig. 1) (Erickson and Blade, 1963).

Age	Formation	Description	Thickness (feet)
Mississippian	Stanley shale	Shale, sandstone and conglomerate.	±3,500
	Hot Springs sandstone.	Sandstone, conglomerate, and shale.	0–200
Mississippian and Devonian.	Arkansas novaculite	Novaculite, calcareous novaculite, shale, sandstone and conglomerate.	100–800
Silurian	Missouri Mountain shale.	Shale, sandstone, quartzite and conglomerate.	50–100
	Blaylock sandstone	Sandstone and shale	0–550
Ordovician	Polk Creek shale	Shale, sandstone, and chert.	25–200
	Bigfork chert	Chert, shale, sandstone, and limestone.	700
	Womble shale	Shale, sandstone, limestone.	250–900

Figure 2: Table describing the stratigraphy of the rocks the MCIC intruded into. Modified from Erickson and Blade (1963).

The MCIC intruded into Paleozoic rocks that had already undergone deformation, just south of the Benton Uplift (Fig. 3). The sedimentary rocks the MCIC intruded into shales, novaculite, sandstones, conglomerates, and chert. Upon intrusion, the igneous complex also metamorphosed the surrounding sedimentary rock, contact metamorphosing the surrounding rocks like novaculite, a cryptocrystalline chert (Keller et al., 1977) and introduced new or unusual minerals like tainiolite (Miser and Stevens, 1938). The Ouachita Mountains, of which these folded rocks are a part of, were deformed due to compression in the middle to late Pennsylvanian. This caused the creation of tightly folded anticlines and synclines (Miser, 1929). Two major synclines and synclinoriums are present in this region of Arkansas, the Ouachita and Mazarn basin. The Mazarn basin is bounded by folds with different trends, the Zigzag Mountains plunge Northeast and the Trap Mountains East-West (Fig. 3). It is initially theorized that the

intrusive igneous activity in the region was due to crustal thinning from an extensional stress regime as the result of the breakup of Pangea ca. 200 Ma (Erickson and Blade, 1963; Williams, 1941).

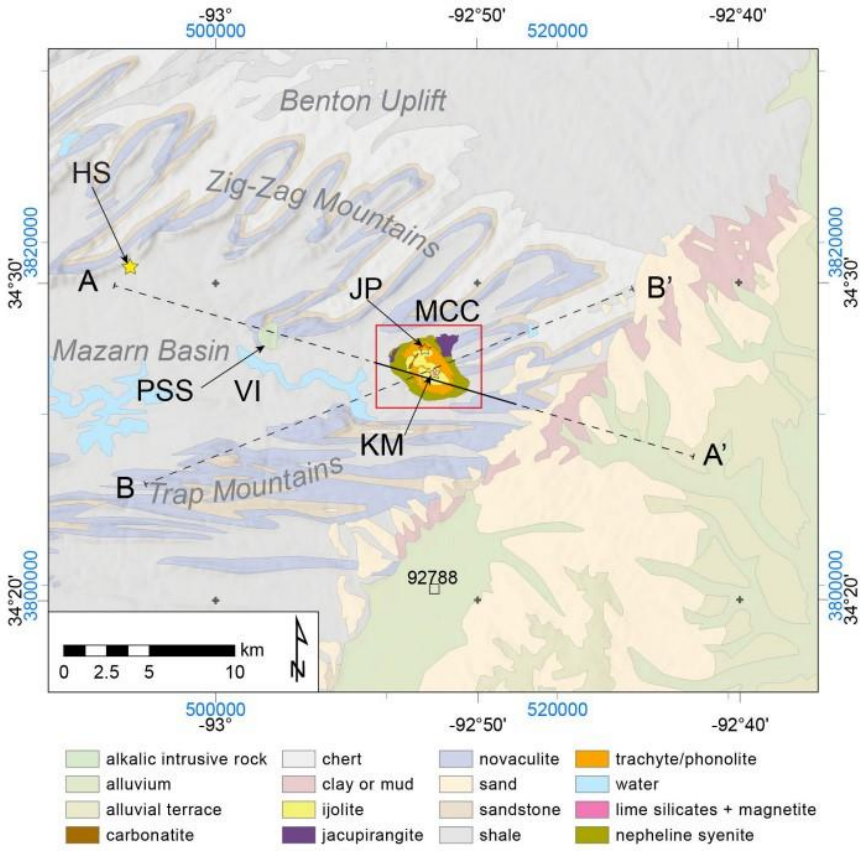

Figure 3: Geologic map of the MCIC and the surrounding area, modified from Amaral (2022). The simplified map of the MCIC (in this figure labeled MCC) is a simplified version of Erickson and Blade's (1963) by Flohr and Ross (1989). Potash Sulfur Springs is denoted as PSS. The map of the surrounding area is adapted from Haley et al. (1993). Dashed lines represent the extent of the data collected for Haley et al. (1993).

Previous Radiometric Data 2.3

Previous geochronologic research has dated the Magnet Cove igneous complex with different methods, however U-Pb, a very robust and precise method, has rarely been applied. Zartman and Howard (1987) used the U-Pb isotope ratios of zircons from Potash Sulfur Springs, another igneous complex in Arkansas (abbreviated as PSS in Fig. 3), that yielded ages from 90 ±

1 – 98 ± 1 Ma. However, there is no zircon reported from the MCIC. There is also no information on perovskite and little on schorlomite being used for geochronology at the MCIC. A single study recently dated MCIC schorlomite by laser ablation (Yang et al, 2018) at 96.4 ± 1.8 Ma, indicating feasibility of using MCIC schorlomite as reference material. Unfortunately, the study gives no details on the exact location and rock type the schorlomite was extracted from. This prohibits the possibility to easily obtain more material, which is a basic requirement for reference materials. Zartman et al. (1967) calculated ages for the garnet ijolite via K-Ar and Rb-Sr of biotite that resulted in initial ages of 97 ± 5 Ma and 99 ± 8 Ma, respectively. The ages were recalculated to account for the new decay constants from Dalrymple (1979) for K-Ar and Nebel et al. (2011) for Rb-Sr. The new ages were calculated as 100 ± 5 Ma for K-Ar and 94 ± 5 Ma for Rb-Sr.

Magmatism in the AAP has been proposed to have occurred in a single distinct pulse from ~110-85 Ma during the subduction of the Farallon plate under the North American plate (Duke et al., 2014). Within this ca. 25 m.y. pulse, there was evolution of the magmas that resulted in decreasing $^{87}Sr/^{86}Sr$ isotope concentrations and increasing εNd values. It is estimated that the carbonatites and ijolites of the MCIC intruded sometime between 103 Ma and 94 Ma (see compilation by Eby & Vasconcelos, 2009), originating from an asthenosphere dominated source. The syenites in the region are estimated to have intruded in a much shorter time frame, between 101.8 and 98.1 Ma (Duke et al., 2014).

The emplacement of the alkaline rocks within the MCIC are hypothesized to be from outside-in, with the outermost ring of phonolite the oldest, and the innermost carbonatite the youngest. Erickson and Blade (1963) stated that the abundance of volatiles and amygdaloidal textures support the hypothesis that the earliest igneous activity was extrusive, which is

represented by the fine-grained phonolites, contrasted with the medium to coarse grained intrusive rocks that make up the rest of the MCIC. Fission-track ages from the phonolites were calculated as 98.4 ± 9.8 Ma from titanite and 98.7 ± 17.8 Ma from apatite (Eby, 1987). Therefore, with uncertainty, it is possible that the extrusive activity occurred in the same Mid-Cretaceous time frame as the intrusive body, which is calculated to occur between 90 ± 9 Ma and 105 ± 10 Ma (Scharon and Hsu, 1969).

No detailed order of emplacement by absolute age of the individual rock types has previously been determined. However, the ijolite and carbonatite core and basin of the complex is considered to be the last rock types to crystallize (Erickson and Blade, 1963).

Chapter 3: Methods

Sample Materials 3.1

Sample Acquisition

Most samples were acquired from the KU Geology department teaching collection. They were originally collected by R. van Schmus during a field trip to the MCIC in 1969, led by M. Bickford and Elliot (Bud) Gillerman (pers. comm. van Schmus, 2022). The perovskite and some kimzeyite samples used for comparison were graciously donated by Mike Howard (Arkansas), and one sample with coarse-grained perovskite was bought on ebay from a mineral shop. Unfortunately, the samples were not documented in detail with their corresponding collection locations. This required in-depth hand sample and thin section petrography to identify the minerals, name the rocks, and be able to locate their general collection area on the geologic map. Sample MC-30 only had thin sections available, and the Ebay perovskite was a hand sample.

Sample Methods 3.2

Sample Petrography and Preparation

The hand samples and thin sections were moved from the teaching collection to the University of Kansas Geology isotope geochemistry laboratory for petrographic investigation and analysis. For analysis, coarse perovskite crystals from a carbonatite sample were broken out of their carbonate groundmass and separated. The individual crystals were then cleaned and embedded in 1-inch epoxy rounds by KU Geology technician Pike Holman (Fig. 4). This round was then placed in the LA-ICP-MS and analyzed while more petrography was conducted on the other samples.

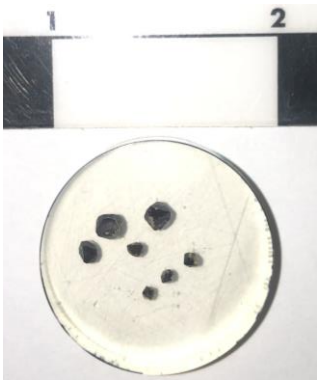

Figure 4: Magnet Cove perovskite mounted in 1-inch round of clear epoxy for analysis by LA-ICP-MS.

After petrographic investigation on standard covered thin sections to identify samples of geochronological interest, the selected hand samples were sent to the KU Geology rock preparation laboratory to be cut into polished sections for LA-ICP-MS for analysis. The only exception being MC-30 due to the lack of a hand sample. For this sample the cover glass of a thin section was removed to access a surface for laser ablation. Hand samples were considered of interest if they had a high presence of identifiable garnet. The composition of rocks from the

MCIC can vary significantly depending on which part of the MCIC it is from. The Ti-rich garnet appears as zoned pale-yellow to black (Fig. 7, 11) or only black (5, 9) minerals in plain polarized light, and is isotropic in crossed polarized light. In reflected light, garnet is a light gray and is usually inclusion rich if from the MCIC. Oxide minerals are very reflective, appearing almost white, distinguishing them from the garnets (Fig. 18, 20, 23, 25).

Sample MC-5 contains many ca. 1mm anhedral to subhedral black garnets and is rich in nepheline and pyroxene, with accessory apatite and titanite (Fig. 5). In hand sample, it is a dark gray to black rock of medium grained composition with a resinous luster (Fig. 6), distinctive of the fine-grained ijolite within the MCIC (Erickson and Blade, 1963).

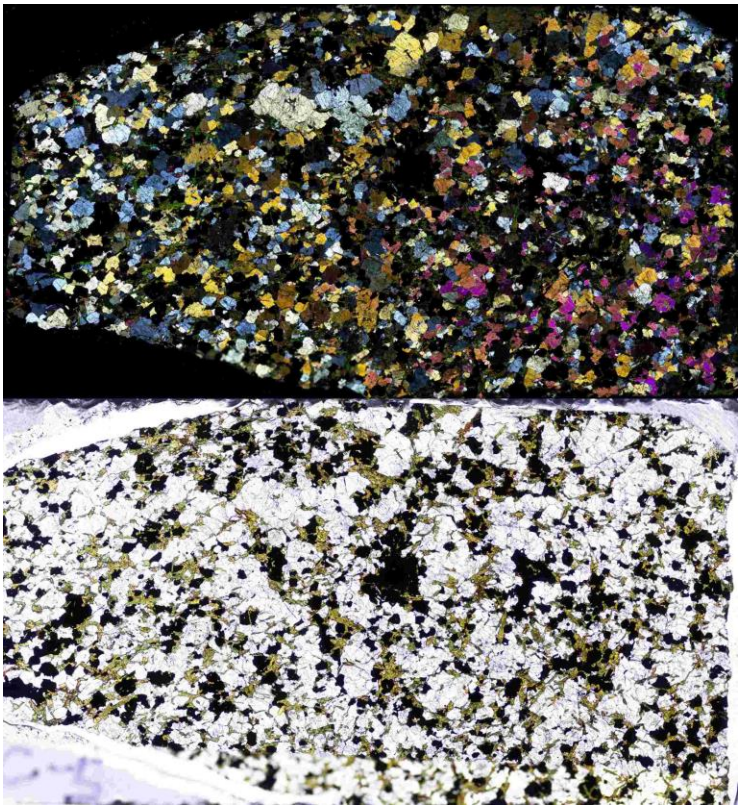

Figure 5: Image of 2.5 cm long MC-5 polished section in crossed (XPL, top) and plain (PPL, bottom) polarized light. The section was unintentionally cut in a wedge, which explains the abnormally high birefringence colors on the right side of the XPL image. Dark minerals in PPL are Ti-rich garnets (schorlomite) and perovskite account for about 20% of the overall modal abundance. Other minerals include clinopyroxene (20%) and nepheline (60%), with accessories biotite, apatite, and titanite. The rock was identified as a fine-grained ijolite.

Figure 6: Photograph of the MC-5 hand sample. Note the distinct resinous luster due to high garnet content. The dark color made it difficult to identify specific minerals in hand sample. The rock weathers to a mottled gray and black.

Sample MC-7 (Fig. 7) is very dark in thin section due to the presence of heavily altered nepheline and leucite. The garnet present is zoned from a yellow andradite to a black schorlomite. Accessory minerals include biotite and apatite. An additional potential mineral present is fluorite, but heavily altered similar to the feldspathoids in the sample. The fluorite occurs as a pale red to pink on the edges of grain boundaries. However, no electron microprobe (EMP) analysis was done to confirm this. In hand sample, the leucite is very easily identifiable as white to light gray 3-5mm phenocrysts. The dark minerals in the hand sample are most likely garnet (Fig. 8). The rock is identified as a garnet-pseudoleucite syenite.

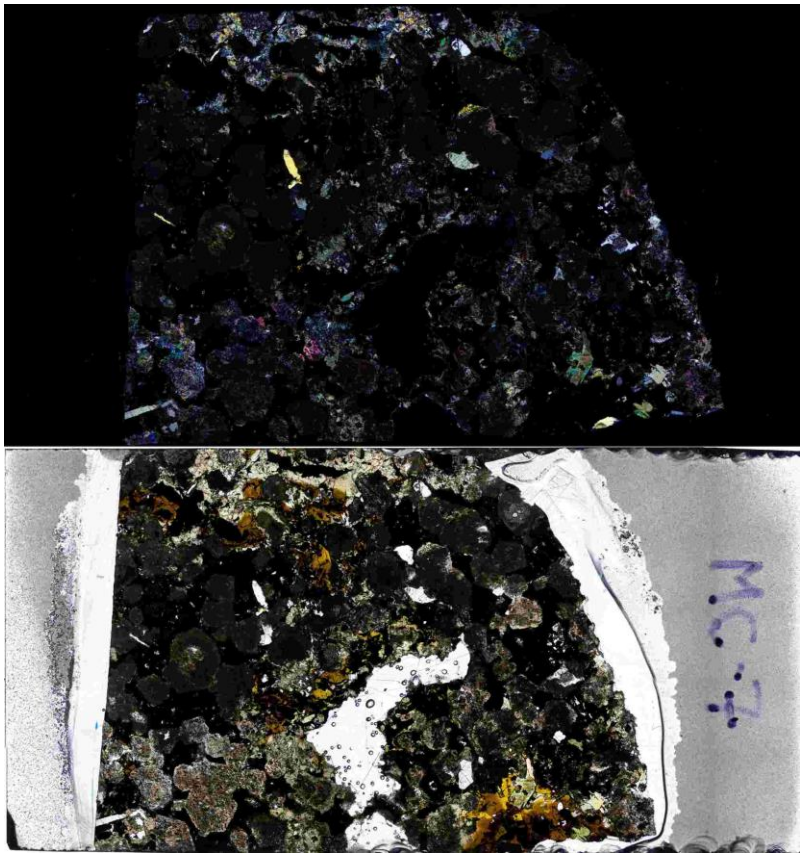

Figure 7: Crossed polarized (top) and plain polarized (bottom) light image of 2.5cm long MC-7 polished section. The garnet that makes up approximately 25% of the modal abundance is strongly zoned from yellow to extremely dark brown in PPL, indicating variations in Titanium content. Other minerals include altered nepheline and leucite (60%) and clinopyroxene (10%) with accessories pale biotite, apatite, and potentially altered fluorite seen as pale pink to red in PPL. The rock was identified as a garnet-pseudoleucite syenite.

Figure 8: Photograph of the MC-7 hand sample. White, pseudocircular (ca. 2mm) minerals are leucite. Much of the rock consists of heavily altered nepheline. Garnet is difficult to identify on a macroscopic scale.

Sample MC-11 appears almost completely black and gray in plain polarized light because of the high abundances of nepheline, leucite, schorlomite garnet, and perovskite (Fig. 9). There are extremely small (<0.1mm) aegirine crystals. The sample has a hairline fracture running through the center, which occurred during preparation. The garnet forms subhedral to euhedral grains (<1mm). The upper right sector of the polished section has a darker, finer grained area that is potentially a residual xenolith, composed chiefly of garnet and diopside post-alteration. The hand sample is gray with up to ~1cm nepheline phenocrysts. Due to the small (<1mm) grain size of the garnets, their identification is difficult in hand sample (Fig. 10). The rock is identified as garnet ijolite.

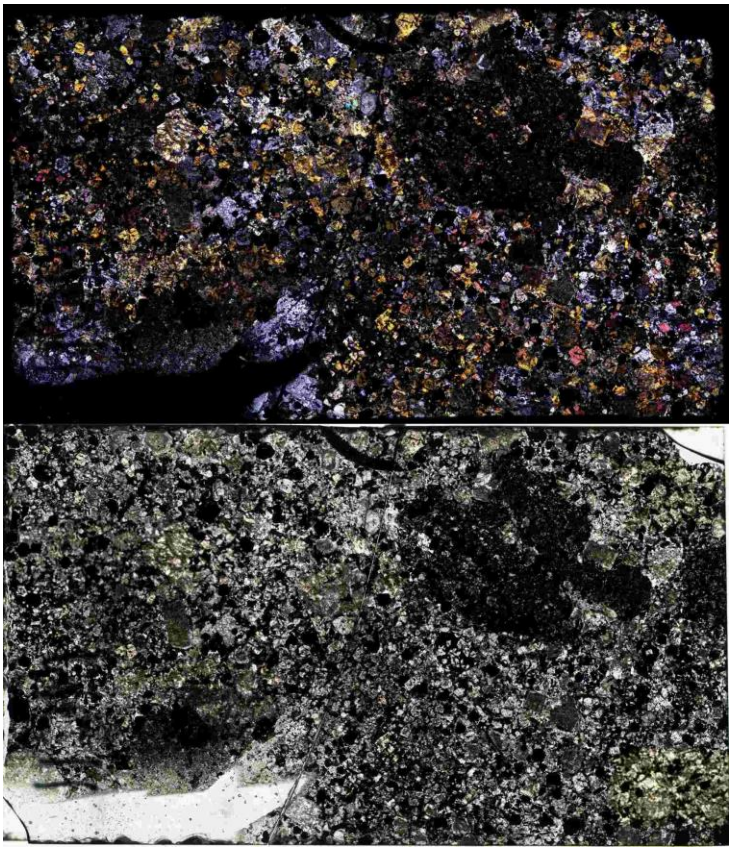

Figure 9: Crossed (top) and plain (bottom) polarized light image of 2.5cm long MC-11 polished section. The garnets in this sample are almost all completely black and constitute about 40% of the rock. Other minerals include nepheline and leucite (50%), and green pyroxene (5%). The accessory minerals include oxides and an extremely birefringent, unidentified mineral that appears heavily altered.

Figure 10: Hand sample image of MC-11. The garnet ijolite can appear dark gray in hand sample. Due to the dark color and small phenocryst size, perovskite and garnet are difficult to differentiate in hand sample. Light gray minerals are nepheline and leucite.

Sample MC-30 is one of the most identifiable rocks of the complex, apart from the carbonatite. The two most abundant minerals are altered nepheline and Ti-garnet. The garnet is very zoned, similar to MC-7 (Fig. 7), and ranges in color from yellow andradite to a completely black or very dark brown schorlomite. One important mineral to note is the presence of perovskite as cores of some of the schorlomite. They are a deep purple-indigo color and are characteristic of the garnet-biotite ijolite (Erickson & Blade, 1963) (Fig. 11). The nepheline is dark gray in PPL and gray with a pale brown tint in XPL, due to the small, less-altered parts of the nepheline crystals. Biotite is moderately abundant in this sample, which is also distinctive of the garnet-biotite ijolite. In some grains, the biotite is cut exactly along its cleavage plane, showing a smooth surface without the basal cleavage normally seen in thin section. Biotite can also occur as Mg rich pale brown or green phlogopite in the ijolites of the MCIC (Erickson and Blade, 1963). Some of the biotite has unusually high birefringence colors. Accessory apatite occurs as euhedral crystals up to 3mm in length.

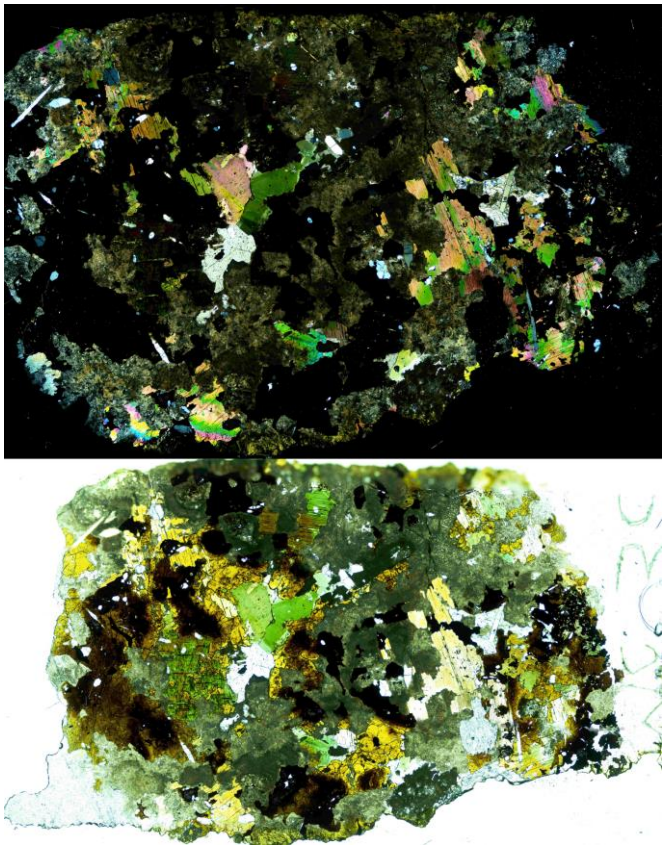

Figure 11: Crossed (top) and plain (bottom) polarized light image of 2.5cm long MC-30 thin section. The garnets of this sample are anhedral and extremely zoned from almost colorless to yellow andradite to very dark brown/almost completely black schorlomite garnet. In some of the grains, perovskite occurs as a blue-purple core. The nepheline in this sample is extremely altered and appears as gray to dark gray. Pale brown to green biotite is present, with the cut occasionally directly along the cleavage plane. Erickson and Blade (1963) also note the presence of phlogopite mica in some places that might be mistaken for biotite. Euhedral apatite is also present as up to 1mm crystals. The modal abundance is 45% nepheline, 30% garnet, 15% biotite, 5% apatite, with accessory minerals of perovskite, phlogopite, calcite, and chlorite.

LA-ICP-MS U-Pb Methodology

Table 1: Data Reporting Table for Perovskite Analysis. Table modified from Horstwood et al. (2016).

Laboratory & Sample Preparation	
Laboratory Name	KU Isotope Geochemistry Laboratory
Sample Type/Mineral	Perovskite
Sample Preparation	Epoxy grain mount (1in)
Imaging	Fluorescence
Laser Ablation System	
Make, Model, & Type	Arf excimer 193nm, Photon Machines Analyte G2, ATL
Ablation Cell & Volume	Helex 2, two-volume cell
Laser Wavelength (nm)	193
Pulse Width (ns)	5
Fluence (J/cm^-2)	2.7
Repetition Rate (Hz)	10
Spot Size µm	35
Sampling Mode / Pattern	Spot
Carrier Gas	He: 1.01 L/min; Ar: 1.1 L/min
Ablation Duration (sec)	30
Cell Carrier Gas Flow (L/min)	Ar: 1.1 L/min
ICP-MS Instrument	
Make, Model, & Type	Thermo Element2 Magnetic Sector Field ICP-MS
Sample Introduction	Meinhard Mixing Bulb
RF Power (W)	1100
Make-up Gas Flow (L/min)	Ar: 1.1 L/min
Sampling Depth	4
Detection System	Single detector, counting, and analog
Masses Measured (Integration time in ms)	206Pb (40), 207Pb(88), 208Pb(8), 232Th(8), 238U(40)
Total Integration Time per Reading (ms)	184
Total Method Time (sec)	47
IC Dead Time (ns)	8
ThO+/Th+ (%)	U/UO <0.2
232Th+/238U+	0.7
Data Processing	
Gas Blank (sec)	17
Calibration Strategy	IR6 for laser induced fractionation, drift, etc.
Reference Material Info	IR6 (Tappe and Simonetti, 2012)
Data Processing Package Used / Correction for LIEF	IGOR PRO, Iolite 2.5
Common-Pb Correction, Composition, and Uncertainty	N/A
Quality Control / Validation	Afrikanda perovskite (Reguir et al., 2010)

The U-Pb decay system was used for the geochronology of this study. To measure the isotope ratios, laser ablation inductively coupled mass spectrometry (LA-ICP-MS) was used, employing a Photon Machines Analyte.G2 193nm excimer laser and Thermo Scientific Element2 mass spectrometer. These are housed at the University of Kansas Isotope Geochemistry Laboratory. The program Chromium 2.4 was used to place spots on each sample and create a standard task file to gather the data. Approximately 40 spots were placed on each sample to be ablated by the laser. The spot locations were chosen based on the transmitted and reflected light capabilities of the laser systems camera. Ablation spots were placed along traverses through the minerals to capture any possible zoning in U-Pb, carefully avoiding visible fractures and alterations. Groups of 6-10 unknowns were bracketed by analyses of NIST SRM glasses and garnet and perovskite reference materials. The laser ablation and ICP-MS parameters used are listed in Tables 1 and 2. Data were processed using IOLITE 2.5 (Paton et al. 2010, 2011) including editing of outliers. For garnet, the measured raw data were corrected to known Pb-Pb values, using NIST SRM614 glass (Jochum et al., 2011). The reference baseline material used to correct the U-Pb fractionation for the garnet was Mali, and the accuracy of the calibration was checked using the Lake Jaco garnet (LJ), both of which were originally dated in Seman et al. (2017). For the perovskite, the reference material for calibration was the Ice River perovskite (IR6) (Tappe and Simonetti, 2012), and the accuracy was checked using Afrikanda perovskites (Afr and EAfr) (Reguir et al., 2010). Concordia plots and age calculations were carried out using the latest version of IsoplotR online (Vermeesch, 2018).

Table 2: Data Reporting Table for Ti-Garnet Analysis. Table modified from Horstwood et al. (2016).

Laboratory & Sample Preparation	
Laboratory Name	KU Isotope Geochemistry Laboratory
Sample Type/Mineral	Ti Garnet
Sample Preparation	Polished thick section (ca. 100µm), and one thin section (MC-30)
Imaging	Reflected light
Laser Ablation System	
Make, Model, & Type	Arf excimer 193nm, Photon Machines Analyte G2, ATL
Ablation Cell & Volume	Helex 2, two-volume cell
Laser Wavelength (nm)	193
Pulse Width (ns)	5
Fluence (J/cm^-2)	2.7
Repetition Rate (Hz)	10
Spot Size µm	85
Sampling Mode / Pattern	Spot
Carrier Gas	He: 1.01 L/min; Ar: 1.1 L/min
Ablation Duration (sec)	30
Cell Carrier Gas Flow (L/min)	Ar: 1.1 L/min
ICP-MS Instrument	
Make, Model, & Type	Thermo Element2 Magnetic Sector Field ICP-MS
Sample Introduction	Meinhard Mixing Bulb
RF Power (W)	1100
Make-up Gas Flow (L/min)	Ar: 1.1 L/min
Sampling Depth	4
Detection System	Single detector, counting, and analog
Masses Measured (Integration time in ms)	206Pb (40), 207Pb(88), 208Pb(8), 232Th(8), 238U(40)
Total Integration Time per Reading (ms)	184
Total Method Time (sec)	47
IC Dead Time (ns)	8
ThO+/Th+ (%)	U/UO <0.2
232Th+/238U+	0.7
Data Processing	
Gas Blank (sec)	17
Calibration Strategy	NIST614 for Pb Calibration, drift, etc.; Mali for U-Pb
Reference Material Info	NIST614 (Jochum et al., 2009); Mali (Seman et al. 2017)
Data Processing Package Used / Correction for LIEF	IGOR PRO, Iolite 2.5
Common-Pb Correction, Composition, and Uncertainty	N/A
Quality Control / Validation	Lake Jaco (Seman et al., 2017)

Laser Ablation Reference Material Data

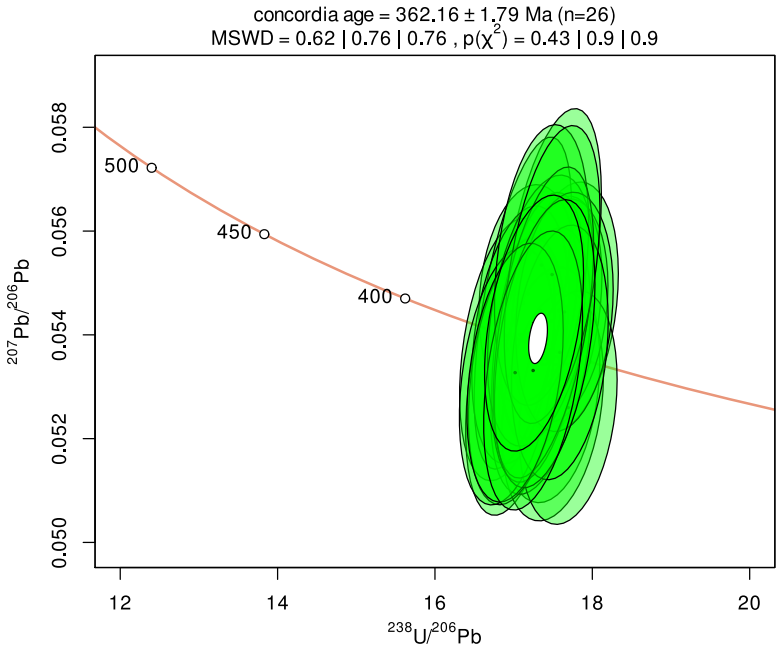

Figure 12: TW-concordia plot diagram for age calibration reference material Ice River (IR6), yielding 362.2 ± 1.8 Ma without statistical outliers. The TIMS age from literature is 361.7 ± 1.0 Ma (Tappe and Simonetti, 2012).

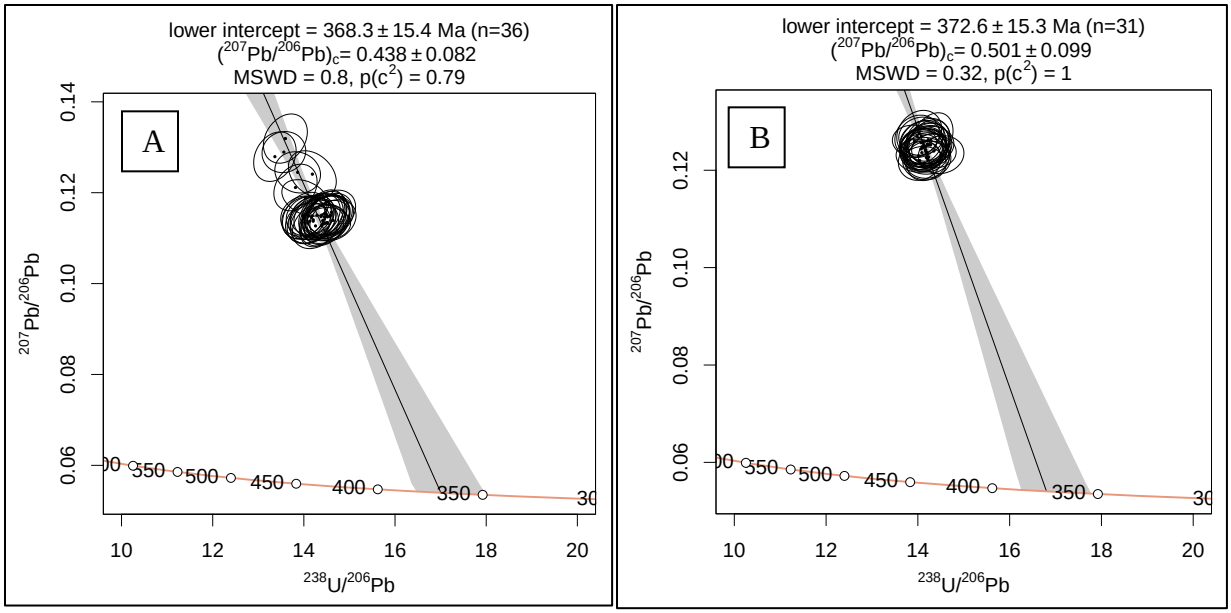

Figure 13: TW-concordia diagrams for age validation reference material Afrikanda (Afr, panel A) and Afrikanda purchased on ebay (EAfr, panel B), anchored at a $^{207}Pb/^{206}Pb$ of 0.50 ± 0.05. The results agree with the LA-ICP-MS age from literature of 371 ± 8 Ma (Reguir et al., 2010).

LA-ICP-MS U-Pb results for the Ice River and Afrikanda perovskites are plotted on TW-concordia diagrams (Fig. 12, 13). The Ice River perovskite resulted in an age of 362 ± 1.8 Ma (Fig. 12), which is identical to the TIMS published age of 361.7 ± 1.0 Ma (Tappe and Simonetti, 2012). The calibration was validated with Afrikanda perovskites, which resulted in ages of 368 ± 15.4 Ma and 372.6 ± 15 Ma (Fig. 13), which is within uncertainty of the published value of 371 ± 8 Ma (Reguir et al., 2010). All controlling parameters used for collection of the perovskite data can be seen in Table 1. Reference material for the perovskite can be seen in Table 3, 4, and 5.

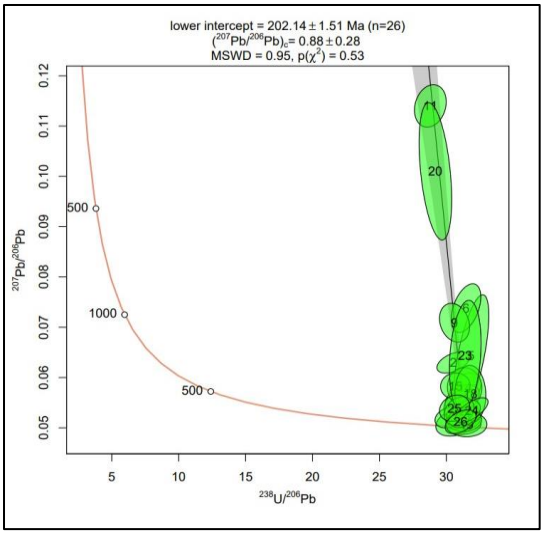

Figure 14: TW-concordia plot diagram for age calibration reference material Mali yields an intercept age of 202.1 ± 1.5 Ma, consistent with the ID-TIMS age from literature of 202 ± 1.2 Ma (Seman et al., 2017).

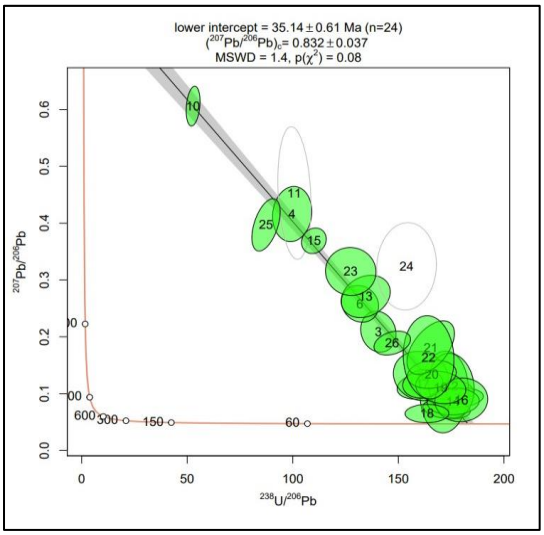

Figure 15: TW-concordia plot diagram for validation reference material Lake Jaco (LJ), yielding an age of 35.1 ± 0.6 Ma. The ID-TIMS age from the literature is 35.0 ± 1.4 Ma (Seman et al., 2017).

LA-ICP-MS U-Pb results for the Mali and Lake Jaco garnets are plotted on TW-concordia diagrams (Fig. 14, 15). The Mali grandite resulted in an age of 202 ± 1.5 Ma (Fig. 14), which is identical to the ID-TIMS published age of 202 ± 1.2 Ma (Seman et al., 2017). The calibration was validated with Lake Jaco grossular garnets from Mexico, giving an age of 35.1 ± 0.6 Ma (Fig. 15) within uncertainty of the published value of 35.0 ± 1.4 Ma (Seman et al., 2017).

All controlling parameters used for collection of the garnet data can be seen in Table 2. Reference material data for garnet is displayed in Table 7 and 8.

Chapter 4: Results

LA-ICP-MS U-Pb Results

Two separate LA-ICP-MS sessions were conducted, one for the perovskite grain mount and another for the Ti-rich garnets, constituting a total of five samples. For the perovskite, 34 analyses were made across the grain with 35μm diameter laser spots. For garnet, 41 analyses were made on MC-5, 43 on MC-7, 44 on MC-11, and 43 on MC-30, all with 85μm diameter spot size. The analyses were made on multiple garnets per sample, along traverses through the visibly color-zoned crystals if possible (Fig. 21, 26). U concentrations are much higher in the perovskite, reaching 289 ppm, compared to the garnets that contain a maximum of 19.5 ppm. Similarly, Th is much higher in the perovskite than the garnets. The garnets tend to be very radioactive, with most of their data plotting with low common Pb and high U-Pb ratios. There is a loose correlation between where the samples plot on the TW-concordia and their U concentrations. Generally, the higher the U concentration, the closer to the lower intercept on concordia the data will plot. There is a significant correlation between the color of the garnet and U concentration. Spots ablated on darker garnet grains tend to result in higher U concentrations, and lighter grains result in lower U concentrations. The zoning is only recognizable under transmitted light in thin section and only applies to samples MC-7 and MC-30 (Fig. 21, 26). Samples MC-5 and MC-11 have garnets too dark to notice zoning in thin section, and there is no obvious trend of U zoning from core to rim (Fig. 5, 9). See Tables 9, 10, 11, 12 for garnet data.

MCIC carbonatite perovskite (MCper)

The perovskite grain is rich in inclusions; however, the majority of the analysis locations were placed in a less complex part of the crystal (Fig. 16). Spots were also placed in the more inclusion-rich areas in order to analyze a complete traverse across the grain. Because this was the only perovskite grain studied, there are as yet no other comparisons to make for perovskite from the MCIC carbonatite from this study. The complete traverse of sample MCper can be seen in Figure 13. One analysis yields as much as 30 ppm; however, the average from the spots of the perovskite grain is 13.7 ppm (see Table 6).

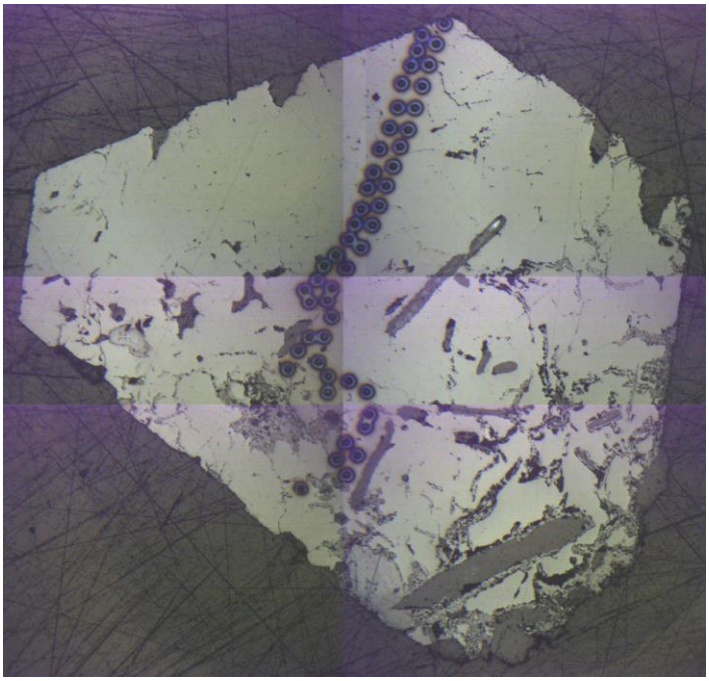

Figure 16: Reflected light image of the traversal of ca. 35μm laser ablation spots on sample MCper. The light color is perovskite, which contains numerous inclusions. The inclusions were deliberately avoided to the best ability when placing spots. The image was created as a mosaic of multiple overview images stitched together, which explains the blue hue of overlapping images.

Of the 34 analyses with 35µm diameter spot size made on the perovskite grain 31 of them were used for the plot after data quality control to calculate a date of 85.5 ± 5.5 Ma (Fig. 17A). The data define a short array in the Tera-Wasserburg diagram, loosely defining an upper intercept with the concordia at a $^{207}Pb/^{206}Pb$ of 0.39 ± 0.7. The uncertainty on this sample is higher than those achieved for the garnet samples of this study, at > 6%. By choosing an anchored $^{207}Pb/^{206}Pb$ of 0.82 ± 0.04 based on data from Duke et al. (2014), the data shifts significantly toward an older date of 100.5 ± 1.7 Ma (Fig. 17B) thus resulting in a much lower uncertainty of 1.7%.

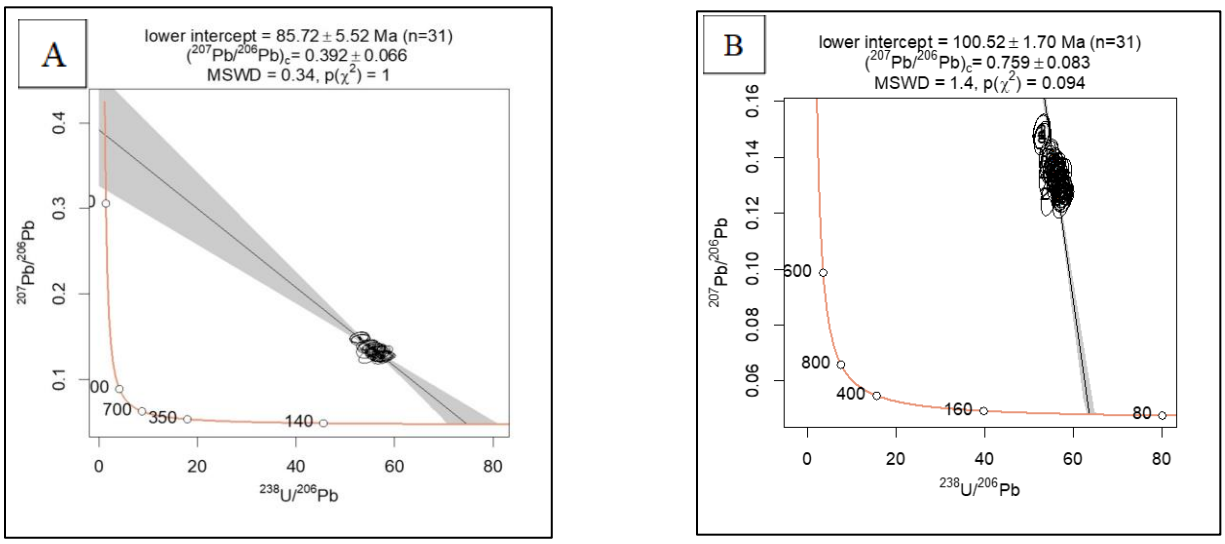

Figure 17: TW-concordia diagrams for U-Pb dating of the MCIC perovskite, sample MCper showing very limited dispersion. [**17A]**: This limited variation in both Pb/Pb and U/Pb ratios produces a low upper concordia intercept and results in a high uncertainty over 6% on the calculated date. [**17B]:** Using the age-corrected 207Pb/206Pb 0.82 from the data of Duke et al. (2014) for the MCIC carbonatite with an assumed uncertainty of 5% (0.04) yields a significantly older date of 100.5 ± 1.7 Ma, with a lower age uncertainty of only 1.7%. Plotted using IsoplotR (Vermeesch, 2018).

MCIC Fine Grained Ijolite (MC-5)

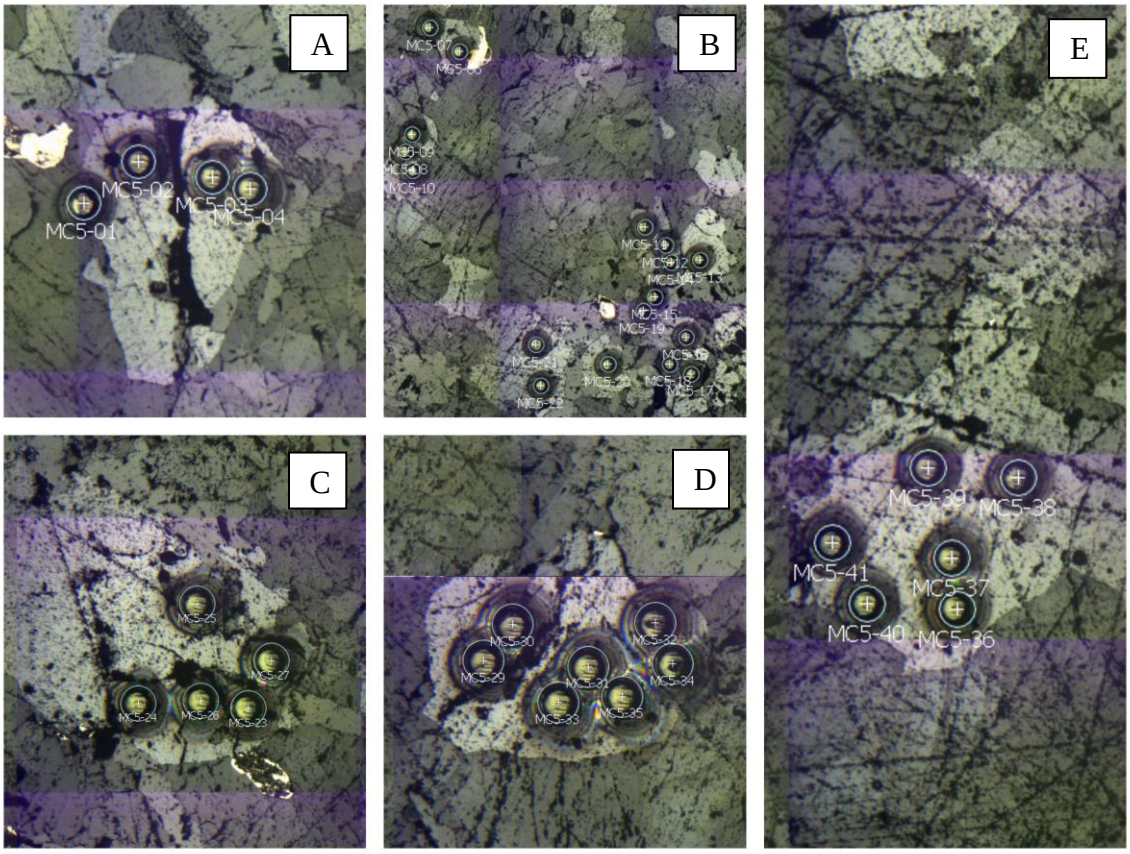

Figure 18: Reflected light images of the traversal of ca. 80µm laser ablation spots on multiple garnets from sample MC-5. **[18A]:** Spots 1-5 at 4x magnification. **[18B]:** Spots 6-22 at 2.95x magnification. **[18C]:** Spots 23-27 at 8x magnification. **[18D]:** Spots 29-35 at 8x magnification. **[18E]:** Spots 36-41 at 4x magnification. The light gray is garnet, which contains numerous inclusions. The inclusions were deliberately avoided to the best ability when placing spots. The image was created as a mosaic of multiple overview images stitched together, which explains the blue hue of overlapping images.

The garnets of sample MC-5 were relatively small and inclusion-rich and therefore acquiring a complete traverse while avoiding them completely was impossible with a spot size of 85µm (Fig. 18). The concordia plot for sample MC-5 (Fig. 19) shows little variation in U concentration and plotted away from the concordia. The discordant data intercepted the concordia at an age of 98.5 ± 1.6 Ma. The analyses 31, 34, and 38 were omitted from the calculation because they plotted off the main trendline or had high uncertainty in Pb isotope ratio

(see Table 9 for data). The U concentration in MC-5 was the second lowest of the four garnet-containing samples studied (4.7 ppm) and ranged from 3.9 ppm to 6.6 ppm. This resulted in a more discordant plot when compared to the other samples. For MC-5 U-Pb data see Table 8.

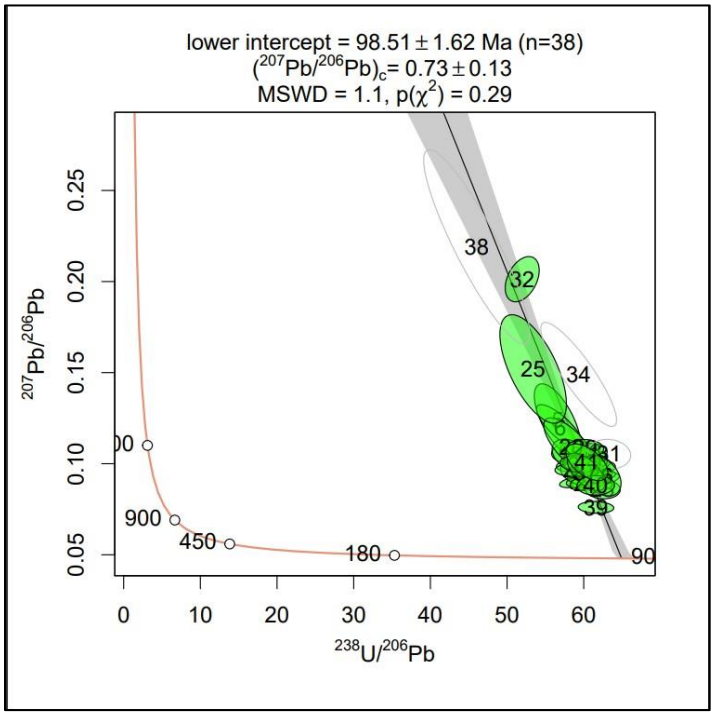

Figure 19: TW-concordia plot diagram for U-Pb dating of the MCIC fine grained ijolite, sample MC-5. Analyses 31, 34, and 38 were deemed outliers most likely due to the ablation of inclusions and removed from the calculation. The isochron has a steep trend and has not been anchored to the y-intercept, and yields a lower intercept age of 98.5 ± 1.6 Ma. Plotted using IsoplotR (Vermeesch, 2018).

MCIC Garnet-Pseudoleucite Syenite (MC-7)

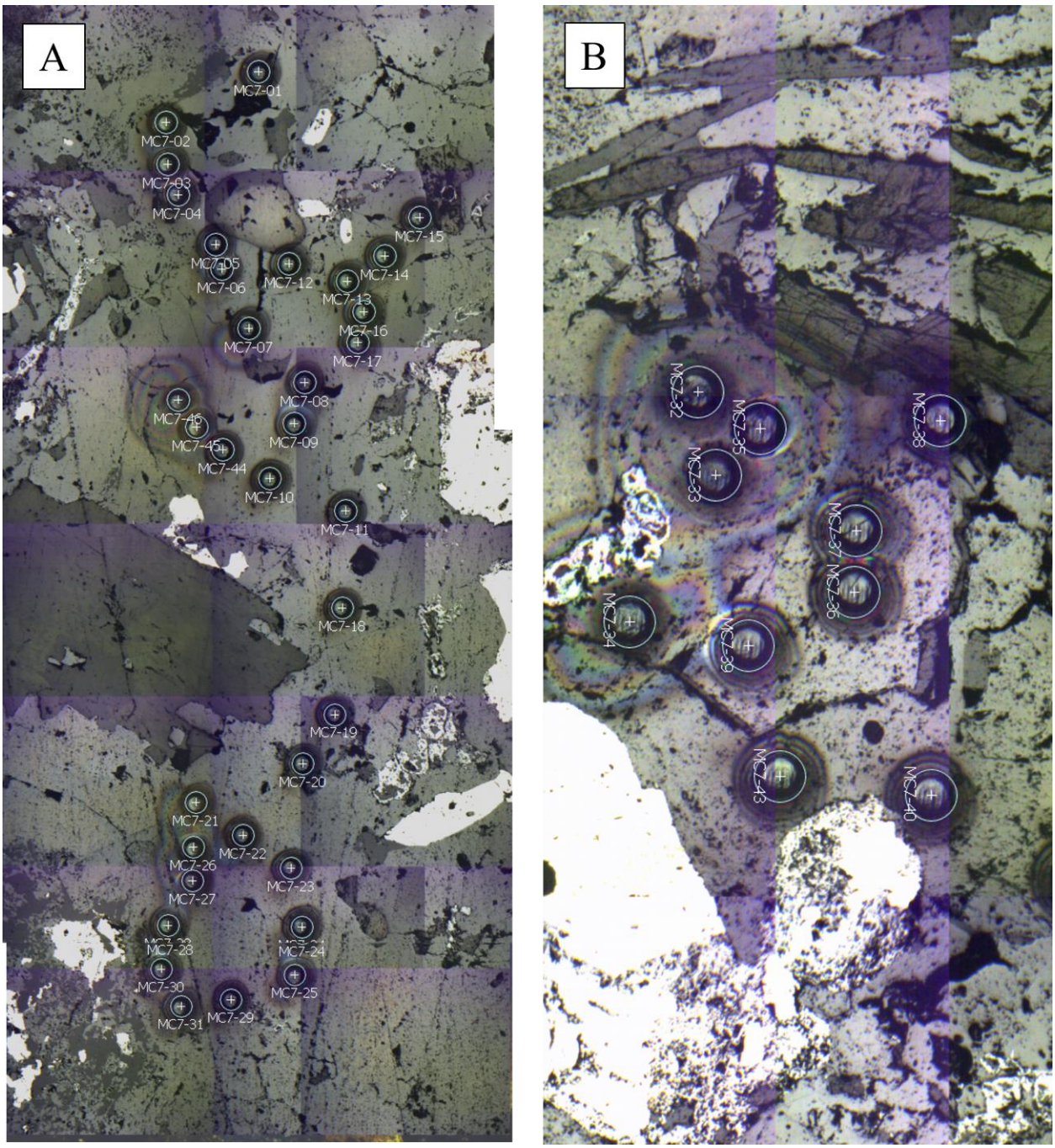

Figure 20: Reflected light images of the traverses of 85 μm laser ablation spots on two large (ca. >1cm) garnets from sample MC-5. **[20A]:** Spots 1-31 at 4x magnification. **[20B]:** Spots 32-43 at 8x magnification. The light gray is garnet, which contains numerous inclusions. The inclusions were deliberately avoided to the best ability when placing spots. The image was created as a mosaic of multiple overview images stitched together, which explains the blue hue of overlapping images.

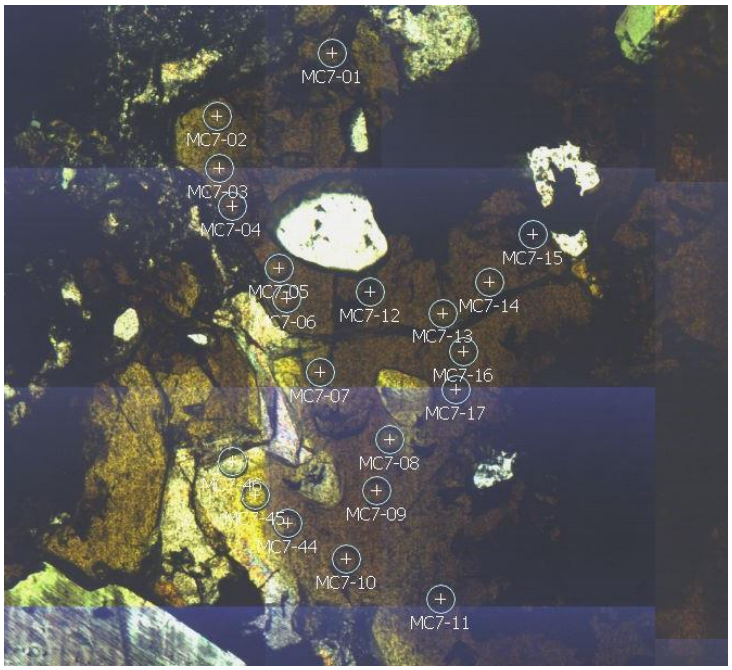

Figure 21: 4x magnification image of a garnet from sample MC-7. Zoning results in a pale brown to yellow to dark brown and results in a trend of increasing concentration. U concentrations (ppm) were as follows: MC7-44 = 4.9; MC7-10 = 6.0; MC7-11 = 10.2.

In sample MC-7, two strongly zoned garnets (Fig. 7, 20, 21) were ablated and analyzed, with the traverses attempting to gather data through all levels of Ti-enrichment. Spot sizes were 85μm. The U concentration of the garnet samples was the highest in MC-7 (7.5 ppm) and also had the widest range, from 0.43 ppm to 19.5 ppm. MC-7 resulted in a disproportionately low Th concentration to high U. It also had the lowest average Pb concentration. Additionally, the $^{207}Pb/^{206}Pb$ ratio was low, and resulted in a loosely defined upper intercept of 1.09 but with an uncertainty of 1.07, or 98%. Spots 11, 35, and 45 control the trajectory of the isochron. Analyses 11 and 45 also had high Pb/Pb uncertainties. Because of the poorly defined upper intercept, the figure was replotted using a $^{207}Pb/^{206}Pb$ of 0.8 ± 0.08, based on the unforced upper intercepts of the other garnet samples. The new diagram maintained a primary age of 101.1 Ma but kept the uncertainty at ± 0.5. A lower intercept of concordia with an age of 101.4 ± 0.5 Ma is well-defined by the majority of the data, and therefore a change in the upper intercept resulted in a minimal date change, from 101.4 ± 0.5 Ma to 101.1 ± 0.5 Ma. For MC-7 U-Pb data see Table 10.

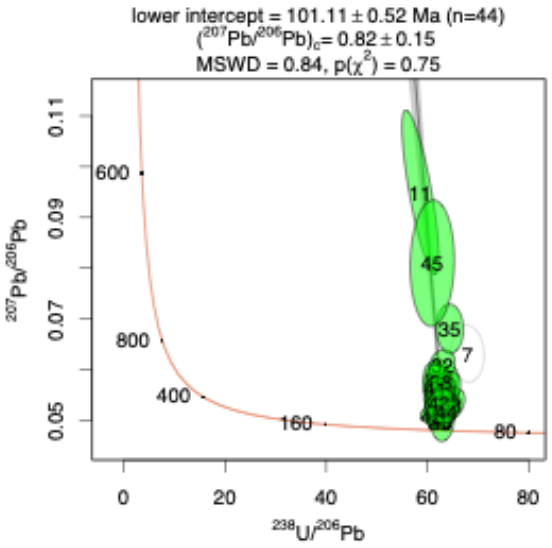

Figure 22: TW-concordia plot diagram for U-Pb dating of the MCIC garnet-pseudoleucite syenite, sample MC-7. Most of the discordant data is concentrated in one particular area of the section. Only spot 7 was deemed an outlier, potentially because it was placed on a pair of observed fractures within the mineral. The Pb isotope ratio was anchored at 0.8 ± 0.08 for the y-intercept, based on the upper intercepts obtained from unforced discordia arrays of the other garnet samples. Plotted using IsoplotR (Vermeesch, 2018).

MCIC Garnet Ijolite (MC-11)

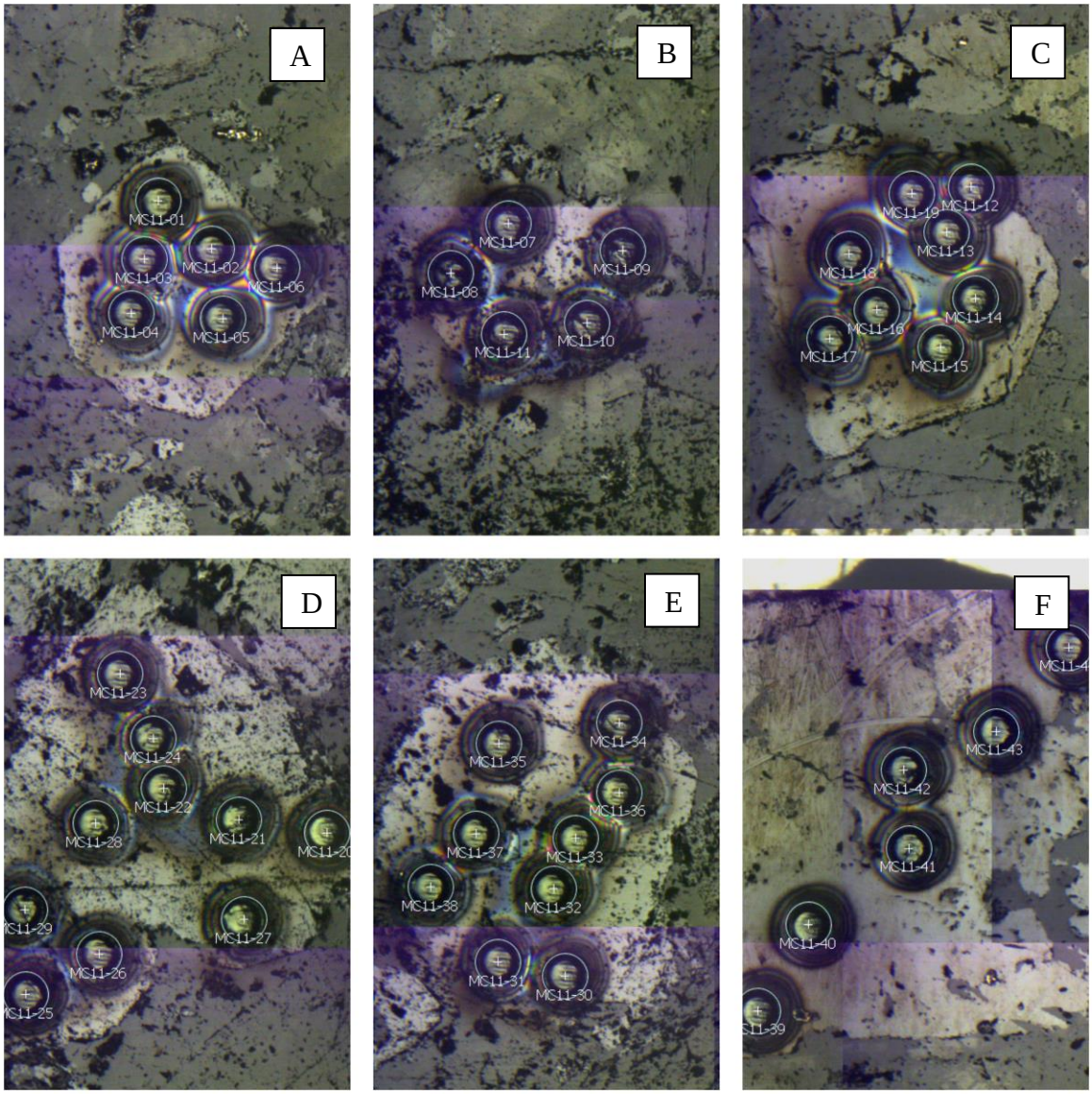

Figure 23: Reflected light images of the traversal of ca. 80µm laser ablation spots on six garnets from sample MC-5. **[23A]:** Spots 1-6 at 8x magnification. **[20B]:** Spots 7-11 at 8x magnification. **[20C]:** Spots 12-19 at 8x magnification. **[23D]:** Spots 20-29 at 8x magnification. **[20E]:** Spots 30-38 at 8x magnification. **[20F]:** Spots 39-44 at 8x magnification. The light gray is garnet, which contains numerous inclusions. The inclusions were deliberately avoided to the best ability when placing spots. The image was created as a mosaic of multiple overview images stitched together, which explains the blue hue of overlapping images. Note spot 8 in [20B], spot 28 in [20D], and spot 30 in [20E]; these spots control the trendline and set the upper intercept.

Sample MC-11 contains subhedral to euhedral medium-sized garnet crystals that are quite rich in inclusions (Fig. 23). Average radioactive U concentrations in MC-11 were the

second highest of the garnet samples (7.1ppm), and ranged from 4.7 ppm to 10.1 ppm, resulting in data that plots nearly concordant. The U-Pb data has moderate spread along the trendline, primarily controlled by spots 8, 28, and 30. MC-11 gave nearly concordant data, with a few analyses controlling the upper intercept, spots 8, 28, and 30. The isochron intersects the x-axis at a U-Pb ratio that corresponds to an age of 98.1 ± 0.6 Ma (Fig. 24). MC-11 provided an upper intercept of a Pb/Pb ratio of 0.79. Spot 8, as seen in Figure 20 below, is within an inclusion rich garnet, and relatively close to the edge of the grain. However, spot 8 lies on the same trajectory as spots 28 and 30, which have very low uncertainties in both ratios associated with them. Spot 28 is in the center of a grain and spot 30 is near the edge, similar to spot 8. Additionally, spots 28 and 30 were on larger grains than that of spot 8 (Fig. 23), indicating that spot 8 is most likely not an outlier and can be included in the data. For MC-11 U-Pb data see Table 11.

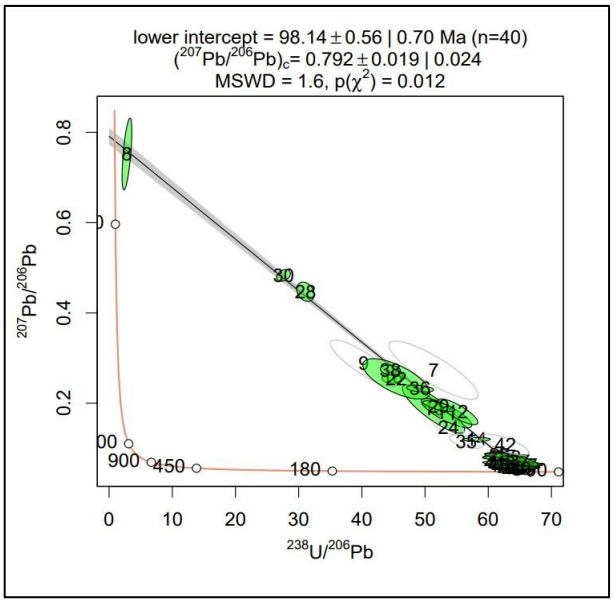

Figure 24: TW-concordia plot diagram for U-Pb dating of the MCIC garnet ijolite, sample MC-11. Spots 7, 9, 24, 35, and 42 were deemed outliers most likely due to the ablation of inclusions and removed from the calculation. Spots 8, 28, and 30 give spread to the data towards the upper intercept of the trendline. The discordia is defined on both the x and y axes by data. Plotted using IsoplotR (Vermeesch, 2018).

MCIC Garnet-Biotite Ijolite (MC-30)

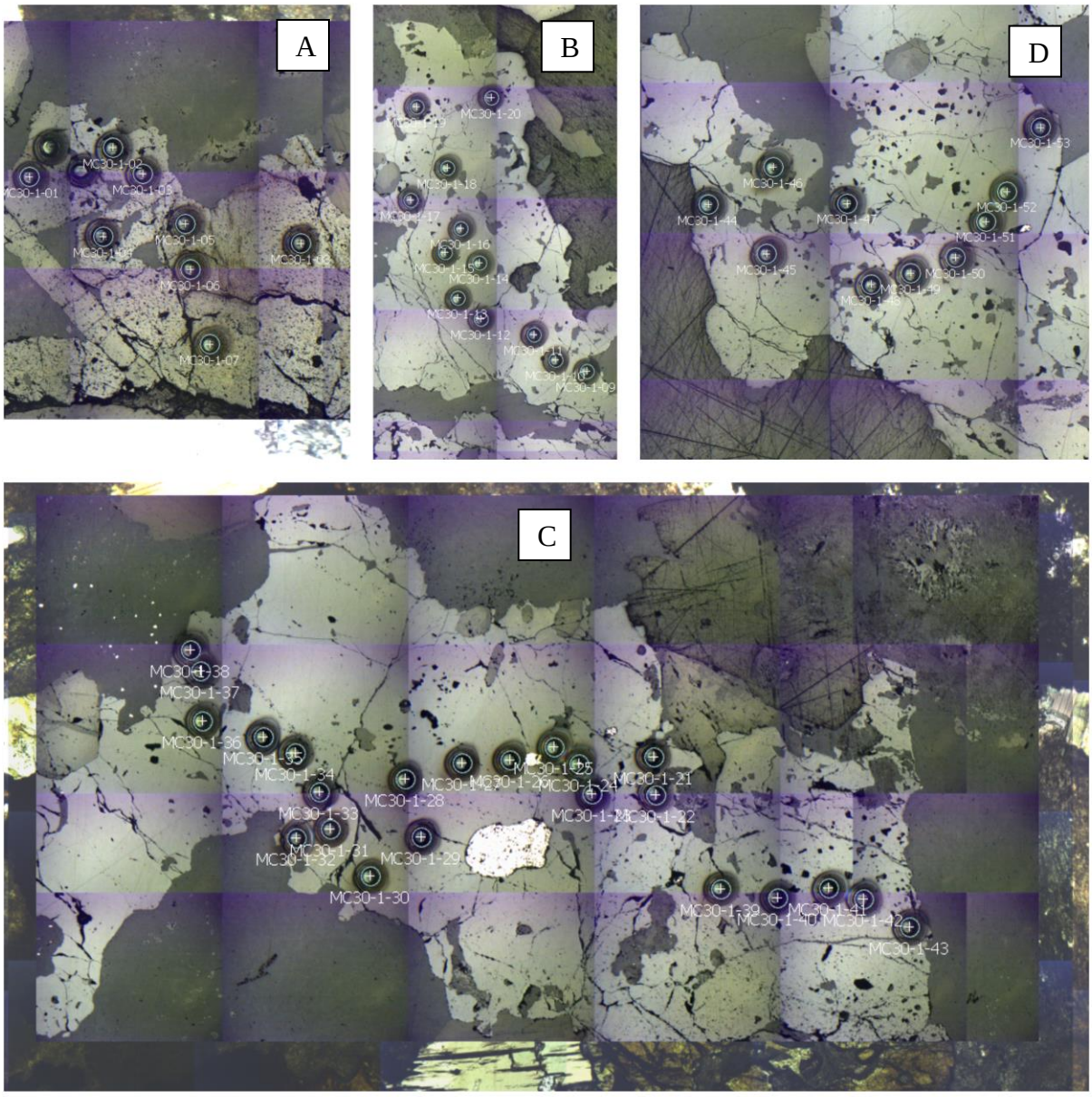

Figure 25: Reflected light images of the traversal of 85µm laser ablation spots on multiple large (>1cm) garnets from sample MC-5. **[25A]:** Spots 1-8 at 4x magnification. **[25B]:** Spots 9-20 at 2.95x magnification. **[25C]:** Spots 21-43 at 2.95x magnification. **[25D]:** Spots 44-53 at 4x magnification. The light gray is garnet, which contains numerous inclusions, particularly in the region of spots 1-8 and 39-43. The inclusions were deliberately avoided to the best ability when placing spots. The image was created as a mosaic of multiple overview images stitched together, which explains the blue hue of overlapping images.

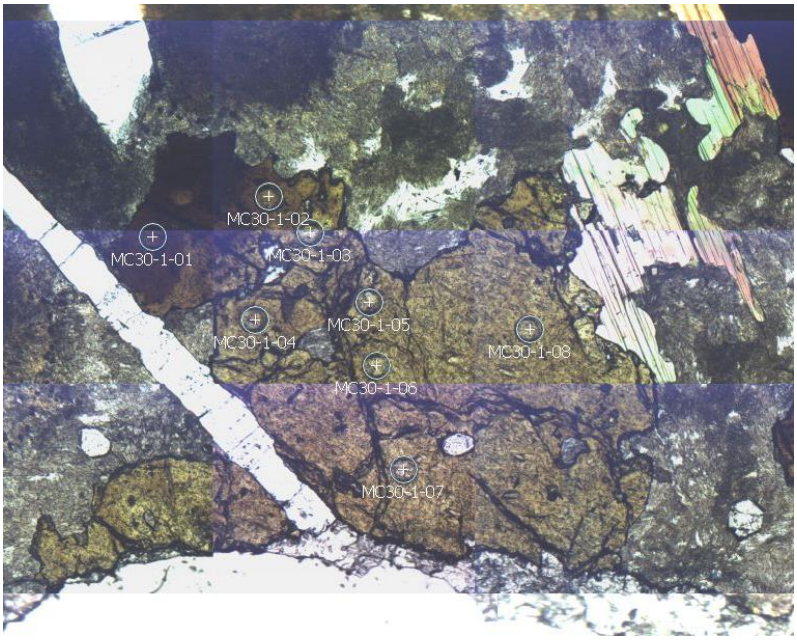

Figure 26: 4x magnification image of a garnet from sample MC-30. Zoning results in a pale brown to yellow to dark brown, and also results in a trend of increasing concentration. U concentrations (ppm) were as follows: MC30-1-08 = 2.6; MC30-1-02 = 3.4; MC30-1-01 = 5.6.

Sample MC-30 contains a high amount of large, zoned garnet (Fig. 25, 26). Multiple large (>1cm) garnets (Fig. 25, 26) were ablated and analyzed, with the traverses aimed at gathering data through all levels of Ti-enrichment. Spot sizes were 85μm (Fig. 25, 26). The data was spread enough in both Pb/Pb and U/Pb space to form a trendline with low uncertainty. The isochron intersects the x-axis with a U-Pb composition that corresponds to an age of 102.8 ± 0.6 Ma (Fig. 27). MC-30 provided a predicted y-intercept of a Pb/Pb ratio of ca. 0.76. There is no single analysis that anchors the isochron on the y-axis, but multiple analyses define a precise array. MC-30 had both the lowest average U and Pb concentration of all the samples used in this study with 3.7 ppm and 0.03 ppm, respectively. The color zoning of the garnet correlated with U, with higher U concentrations in the darker garnet and lower U in the lighter garnet. Spots MC30-1-08, MC30-1-02, and MC30-1-01 show increasing concentrations of U from light to dark, with MC30-1-08 at 2.6 ppm and MC30-1-01 at 5.6 ppm. The majority of the data is near concordant, due to a high U-Pb ratio. Although, spots 2, 5, 11, and 44 controlled the trajectory of the

isochron. The omitted spots had little to no effect on the lower intercept of the line and its uncertainty if they were included or excluded. For MC-30 U-Pb data see Table 12.

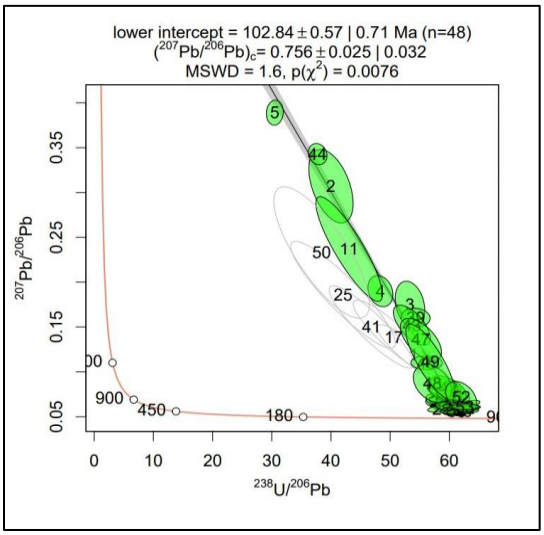

Figure 27: TW-concordia plot diagram for U-Pb dating of the MCIC garnet-biotite ijolite, sample MC-30. The majority of the data is concentrated in one region that is discordant. Spots 1, 17, 25, 41, and 50 were deemed outliers most likely due to the ablation of inclusions or ablating a different mineral and were therefore omitted. The isochron has a steep trend and no anchor on the y-intercept. The spots are moderately spread across the trendline, with spots 2, 5, 11, and 44 controlling its trajectory. Plotted using IsoplotR (Vermeesch, 2018).

Chapter 5: Discussion

Each sample analyzed had high enough U and Pb concentrations to calculate a date. The analyzed perovskite from the MCIC carbonatite had little dispersion in the TW-diagram, and the result is therefore somewhat dependent on the upper intercept. The un-anchored data define an upper intercept of 0.39 ± 0.07. The uncertainty on the date is higher than 6%, and therefore not ideal as a U-Pb LA-ICP-MS reference material. The date obtained of 85.7 ± 5.5 Ma is broadly consistent with the younger end of the range of the first major pulse of midcontinent Mid to Late Cretaceous magmatism according to Duke et al. (2014), which occurred between 110 – 85 Ma. According to Erickson and Blade (1963) the carbonatite was intruded last of all the MCIC rocks, consistent with a younger date than the other intrusives of MCIC. However, no previous

geochronological studies of the MCIC resulted in ages this young, even within the corresponding calculated uncertainty (e.g. Zartman et al. 1967; Eby & Vasconcelos, 2009; Yang et al. 2019), except the lower end of Scharon and Hsu (1969) age of 90 ± 9 Ma. Duke et al. (2014) also indicated that *carbonatite* magmatism in Arkansas occurred between 103 and 94 Ma, based on the Eby & Vasconcelos (2009) compilation of the timing magmatism of Magnet Cove, which is based on previous radiometric studies involving K-Ar and Rb-Sr dating of biotite (Zartman et al., 1967) and whole rock (Baldwin and Adams, 1971), Ar-Ar dating of biotite (Baksi, 1997)) and fission-track dating of apatite and titanite (Arne, 1992; Eby and Vasconcelos, 2009; Scharon and Hsu 1969). This would mean the data from this study constitutes a younger magmatic pulse that formed the MCIC carbonatite. However, the $^{207}Pb/^{206}Pb$ value was unusually low and was instead anchored at 0.82, which provides a date much closer to both the previous estimates and the other rocks of this study, at 100.5 ± 1.7 Ma. The value of 0.82 was calculated from the Duke et al. (2014) whole rock isotope data for the carbonatite, and is also close to the $^{207}Pb/^{206}Pb$ of the garnets of this study, which give values of 0.73, 0.76, and 0.79. A better upper intercept estimate may also be obtained by analyzing cogenetic low-U minerals in the carbonatite, such as calcite or apatite, which may resolve the issue with the date seeming to be too young.

The dates obtained from the MCIC titanium garnets have uncertainties between 0.5 and 1.6 Ma. The calculated dates range from the oldest at 102.8 ± 0.6 Ma to the youngest at 98.1 ± 0.6 Ma. This supports the theory proposed by Duke et al. (2014) that there was a slightly older pulse of magmatism, creating the Arkansas syenites from 101.8 Ma to 98.1 Ma. The only syenite that was utilized in this study was sample MC-7, a garnet-pseudoleucite syenite dated at 101.4 ± 0.8 Ma.

The three other garnet samples used in this study were variations of the MCIC ijolites, yielding 102.8 ± 0.6 Ma (MC30), 98.5 ± 1.6 (MC5) and 98.1 ± 0.6 Ma (MC11). The ages of

ijolites from Magnet Cove were previously determined with apatite and titanite fission track ages by Eby and Vasconcelos (2009) at approximately 96 ± >7 Ma, Ar-Ar of biotite by Baksi (1997) at 94.4 ± 0.2 Ma, and Rb-Sr of biotite by Zartman et al. (1967) at 102 ± 8 Ma. All ages from this study can be reasonably placed within the timeline of central Cretaceous Arkansas alkalic magmatism. Each date calculated in this study is more precise than most previously published dates, and obtained with a more robust geochronometer. With this higher precision, the new garnet dates fall into two distinct groups. The garnet from the MC7 syenite, MC30 ijolite, and the perovskite from the carbonatite form an older group between 102.8 ± 0.6 Ma and 100.5 ± 1.7 Ma. However, it is important to note that when including uncertainty, the perovskite and oldest garnet dates do not overlap (0.05 Ma disparity remains). This can indicate a separation in magmatism timing between the garnet-biotite ijolite and the carbonatite. This date can be interpreted as the time in which carbonatite magmatism began in the AAP. Whereas the fine grained ijolite and the garnet ijolite with dates of 98.5 ± 1.6 (MC5) and 98.1 ± 0.7 Ma (MC11) form a younger group with an average age of 98.6 ± 0.6 Ma that have overlapping uncertainties. The ijolites are in contact with each other within the MCIC (see Appendix C for detailed geological map of Erickson and Blade, 1963). This would indicate two magma pulses separated by approximately 3 m.y, and potentially a third at ~100 Ma that initiated the formation of the carbonatite. It is important to note that the younger rocks are finer-grained, meaning their grain size could have been a result of intruding into colder material, like already emplaced igneous rocks.

The results for the younger group are close to the slightly younger schorlomite age determined by Yang et al. (2019) of 96.5 ± 1.2 Ma. The overall timeline supports the hypothesis by Duke at al. (2014) that the alkalic magmatism of Magnet Cove occurred in conjunction with

the second pulse of the kimberlite magmas of Kansas (Fig. 28), that are also proposed to have occurred from mantle upwelling during the Mid-Cretaceous (Heaman et al., 2004; Meyer, 1976). However, based on the findings of this study, some MCIC magmatism specifically occurred for only a brief period at the start of magmatism in this area, between ca. 98 and 103 Ma (Fig. 28), originating from an enriched (low $^{87}Sr/^{86}Sr$ and high εNd values) asthenosphere-dominated magmatic source (Fig. 29), versus the kimberlites of Kansas that are proposed to have occurred continuously from 110-85 Ma (Duke et al., 2014).

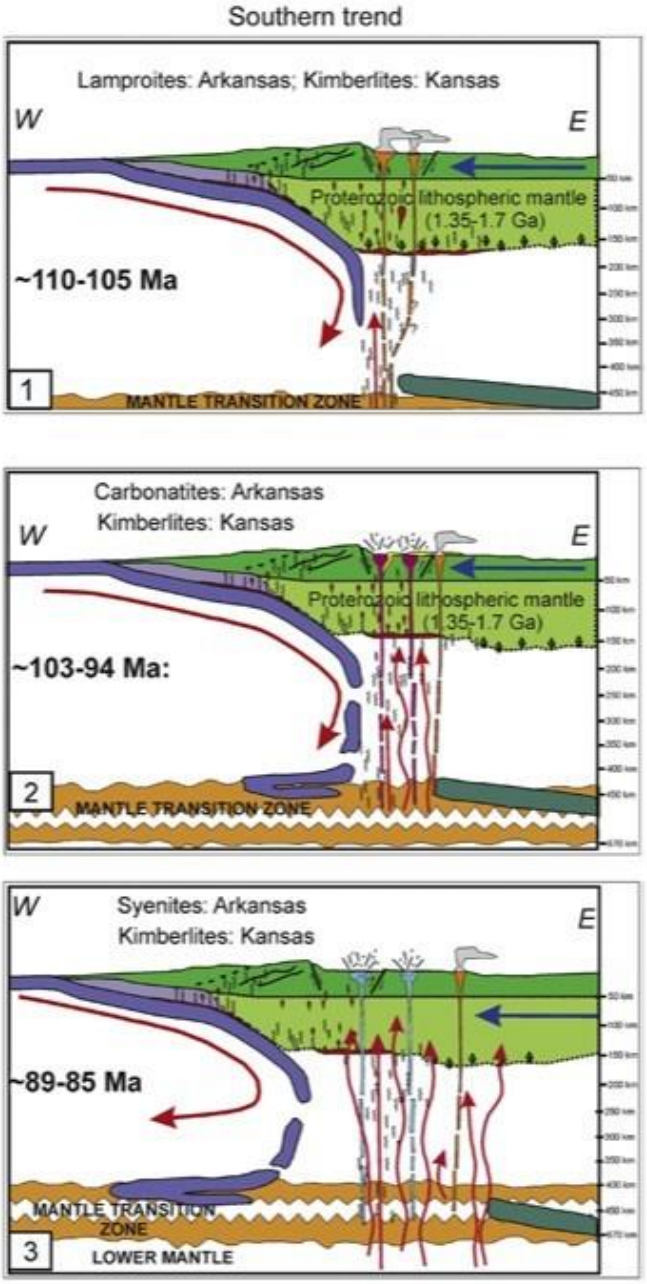

Figure 28: Tectono-magmatic sequence for the first three pulses of midcontinent magmatism. Original figure from Duke at al. (2014). Figure was modified to only include the time slices relevant to this study. The cross-section trends N40°W, from Louisiana to Alberta. Red arrows: mantle flow patterns; Blue arrow: movement direction of North American Plate; orange intrusions are lamproite and kimberlite magmas and lavas; Dark pink intrusions are carbonatites; Light blue intrusions are syenites and nepheline syenites. *1:* (110-105 Ma) Lamproitic volcanism occurred in Arkansas, while kimberlitic volcanism occurred in Kansas. *2:* (103-94 Ma) First pulse of enriched magma, indicating a much more asthenosphere dominated source. This is when Magnet Cove most likely intruded as the carbonatites, ijolites, and nephelinites all point to this time. In Kansas, kimberlite magmatism continued. *3:* Continued magmatism caused the intrusion of syenites in Arkansas. Kimberlite magmatism continued in Kansas until ~85 Ma.

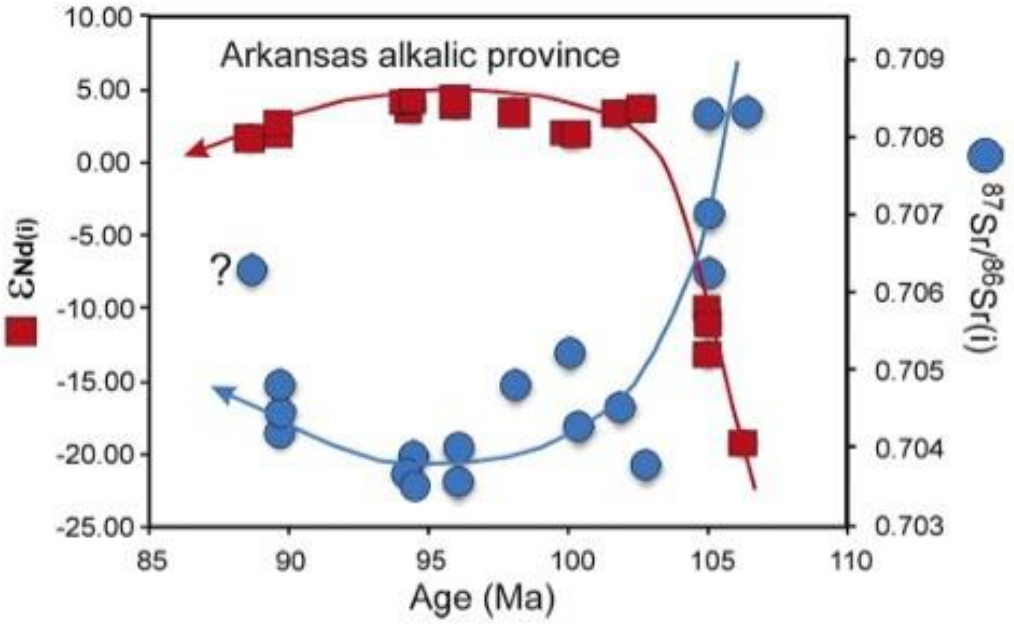

Figure 29: Figure showing the $^{87}Sr/^{86}Sr$ ratios (blue circles) and εNd values (red squares) vs. time for the Arkansas Alkalic province. Both trends show a lithospheric source during the earliest stages of magmatism, before ~105Ma. At ~103Ma the source dramatically changes to more asthenosphere dominated.

Chapter 6: Conclusions and Future Work

The Magnet Cove Igneous Complex contains and is famous for a variety of uncommon rock types. This study was able to determine radiometric ages of a set of ijolite samples, syenites, and the central carbonatite (Fig. 1). The date calculated from the perovskite resulted in a significantly younger age due to low $^{207}Pb/^{206}Pb$. However, if the value was anchored at a calculated 0.82 value, it results in an age more consistent with previous studies and the garnets of this study, 100.5 ± 1.7 Ma. The garnet ages ranged from 102.8 ± 0.6 Ma from the garnet-biotite ijolite (MC-30) to 98.1 ± 0.6 Ma from the garnet ijolite (MC-11). These LA-ICP-MS ages are consistent with the fission track, K-Ar, and Ar-Ar, and LA-ICP-MS ages of previous studies, but with a lower uncertainty, which opens up the possibility of constructing a more detailed intrusive history with more samples. The garnet-pseudoleucite syenite (MC-7) gave an age younger than

the garnet-biotite ijolite (MC-30), despite it occurring in the outermost ring of the complex. This indicates either that this study did not determine the order of emplacement correctly for the individual rock types, or that previous radiometric results date a cooling sequence instead of an emplacement sequence. Additionally, no rocks from the intermediate ring were analyzed in this study (phonolites, trachytes, etc.). The garnets contained high enough concentrations of U-Pb to acquire ages, however more work needs to be done to confirm their potential as reference material, partly because they occur in complex overgrowth textures on earlier minerals that are not amenable to easy mineral separation.

In terms of reference material capabilities, the results on the MCIC perovskite are inconclusive. The perovskite had such little distribution on the T-W diagram and was significantly discordant, however, that the initially obtained uncertainty makes it not ideal as a U-Pb LA-ICP-MS reference material. The perovskite is easy to extract, however, making the continuation of studying the perovskite from the MCIC still feasible. Because only one grain was analyzed, this may have been an outlier and there is no other data to compare it to. Therefore, there is not enough data to completely discount or accept its ability to be used as reference material, especially when considering the new age calculated with an anchored $^{207}Pb/^{206}Pb$. The garnets from the MCIC have a much higher capability to be used in future geochronological studies. The Uranium content was high, and they yielded consistent ages. However, it again falls short due to quantity of data. Only one session was conducted for 4 different rock types, which are already hypothesized to be emplaced at slightly different times. If more analyses were conducted across the same rock type, multiple times, there could be high prospects for utilization as reference material. However, reference materials need to be easily accessible and extractable, and the garnets of the MCIC can occur as rims and reactions, unable to be extracted from the

host rock, like in samples MC-7 and MC-30. Some garnets from the MCIC, like those in MC-5 and MC-11, are more euhedral and can be identified in thin sections. This increases their feasibility as future reference materials. Due to the mineralogical complexity of the area and lack of documentation about the acquired samples, most of the research time was dedicated to petrographic analysis and not to data collection.

Future work can include fieldwork involved with the collection of more samples and their exact location mapped. The abundance of Ti-rich and schorlomite garnet throughout the complex makes collection of garnet-rich samples easy, however there may be restrictions on what is accessible due to private ownership and economic interest in the REE. Electron microprobe (EMP) can play a vital role in the identification and further detailed characterization of some minerals. Some of the rocks involved in this study contain rare minerals that lack proper identification based on petrographic microscope observations alone. Detailed EMP analysis can identify the minerals and help streamline the petrographic analysis process as well as potentially provide information for other mineralogical studies. More analytical sessions beyond the scope of this project will need to be conducted on multiple rock types to properly evaluate the garnet and perovskite from the MCIC as reference material.

References

Amaral, C.M., 2022, Structural Interpretation of an Alkaline-Carbonatite Complex Using Gravity and Magnetic Methods at Magnet Cove, Arkansas. [thesis]: Graduate Theses and Dissertations.

Amaral, C.M. and Lamb, A.P., 2019, Structural interpretation of an Alkaline-Carbonatite Complex at Magnet Cove, Arkansas using gravity and magnetic methods: AGU Fall Meeting Abstracts, v. 2019, p. GP33B-0748.

Arne, D.C., 1992, Evidence from apatite fission-track analysis for regional Cretaceous cooling in the Ouachita Mountain fold belt and Arkoma Basin of Arkansas: AAPG bulletin, v. 76, no. 3, p.392-402.

Aysal, N., Guillong, M., Bayanova, T., Fukuyama, M., Leonard, N., Yılmaz, İ., Varol, E., Tükel, F.Ş., Kadıoğlu, Y.K., Hanilçi, N. and Uzun, F., 2023 in press, A new natural secondary reference material for garnet U-Pb dating by TIMS and LA-ICP-MS: Geostandards and Geoanalytical Research.

Baksi, A.K., 1997, The timing of Late Cretaceous alkalic igneous activity in the northern Gulf of Mexico basin, Southeastern USA: The Journal of Geology, v. 105, no. 5, p. 629–644, doi: 10.1086/515966.

Baldwin, O.D. and Adams, J.A.S., 1971, K40/Ar40 Ages of alkalic igneous rocks of Balcones fault trend of Texas: Texas Journal of Science, v. 22, no. 2-3, p. 223.

Burisch, M., Gerdes, A., Meinert, L.D., Albert, R., Seifert, T. and Gutzmer, J., 2019, The essence of time–fertile skarn formation in the Variscan Orogenic Belt: Earth and Planetary Science Letters, v. 519, p. 165-170.

Brookins, D.G., 1970, The kimberlites of Riley County, Kansas: Kansas Geological Survey.

Brookins, D.G. and Naeser, C.W., 1971, Age of emplacement of Riley County, Kansas, kimberlites and a possible minimum age for the Dakota Sandstone: Geological Society of America Bulletin, v. 82, no. 6, p. 1723-1726.

Chen, K., Shao, Y.J., Zhang, J.K., Zhang, Y., Tan, H.J., Zhang, Y.C. and Liu, Z.F., 2022, Garnet U-Pb geochronology and geochemistry reveal deposit types and fluid evolution: An example from the Dongguashan Cu-Au deposit, eastern China: Ore Geology Reviews, v. 145, p. 104883.

Cox, R. T.; and Van Arsdale, R. B. 1997, Hotspot origin of the Mississippi embayment and its possible impact on contemporary seismicity: Eng. Geol., vol. 46, p. 201-216.

Cox, R. T. and Van Arsdale, R.B., 2002, The Mississippi Embayment, North America: a first-order continental structure generated by the Cretaceous superplume mantle event: J. Geodyn, v. 34, p. 163-176.

Dalrymple, G.B., 1979, Critical tables for conversion of K-Ar ages from old to new constants: Geology, v. 7, no. 11, p. 558-560.

Duke, G.I., Carlson, R.W., Frost, C.D., Hearn, B.C., and Eby, G.N., 2014, Continent-scale linearity of kimberlite–carbonatite magmatism, mid-continent North America: Earth and Planetary Science Letters, v. 403, p. 1–14, doi: 10.1016/j.epsl.2014.06.023.

Duncan, R. A., 1984, Age progressive volcanism in the New England seamounts and the opening of the central Atlantic Ocean: J. Geophys. Res., vol. 89, p. 9980–9990.

Eby, G.N., and Vasconcelos, P., 2009, Geochronology of the Arkansas Alkaline Province, Southeastern United States: The Journal of Geology, v. 117, no. 6, p. 615–626, doi: 10.1086/605779.

Erickson, R.L., and Blade, L.V., 1963, Geochemistry and petrology of the alkalic igneous complex at Magnet Cove, Arkansas: Professional Paper, doi: 10.3133/pp425.

Flohr, M.J., 1994, Titanium, vanadium, and niobium mineralization and alkali metasomatism from the Magnet Cove Complex, Arkansas: Economic Geology, v. 89, no. 1, p. 105–130, doi: 10.2113/gsecongeo.89.1.105.

Flohr, M.J., and Howard, J.M., 1995, Geochemical data of alkaline igneous rocks and carbonatites, Potash Sulphur Springs Igneous Complex, Arkansas: Open-File Report, doi: 10.3133/ofr95836.

Flohr, M.J.K., and Ross, M., 1989, Alkaline igneous rocks of Magnet Cove, Arkansas; metasomatized ijolite xenoliths from Diamond Jo Quarry.: American Mineralogist , v. 74, no. 1-2, p. 113–131.

Flohr, M.J.K., and Ross, M., 1990, Alkaline igneous rocks of Magnet Cove, Arkansas: Mineralogy and geochemistry of Syenites: Lithos, v. 26, no. 1-2, p. 67–98, doi: 10.1016/0024-4937(90)90041-x.

Haley, B.R.; assisted by Glick, E.E., Bush, W.V., Clardy, B.F., Stone, C.G., Woodward, M.B., and Zachry, D.L., 1993, Geologic Map of Arkansas: U.S. Geological Survey, Reston, Virginia, USA

Heaman, L.M., Kjarsgaard, B.A., and Creaser, R.A., 2004, The temporal evolution of North American kimberlites: Lithos, v. 76, no. 1-4, p. 377–397, doi: 10.1016/j.lithos.2004.03.047.

Jochum, K.P., Weis, U., Stoll, B., Kuzmin, D., Yang, Q., Raczek, I., Jacob, D.E., Stracke, A., Birbaum, K., Frick, D.A. and Günther, D., 2011, Determination of reference values for NIST SRM 610–617 glasses following ISO guidelines: Geostandards and Geoanalytical Research, v. 35, no. 4, p. 397-429.

Keller, W.D., Viele, G.W. and Johnson, C.H., 1977, Texture of Arkansas novaculite indicates thermally induced metamorphism: SEPM Journal of Sedimentary Research, v. 47, no. 2, p. 834-843. doi: 10.1306/212f7266-2b24-11d7-8648000102c1865d.

Jung, S. and Mezger, K., 2003, U-Pb garnet chronometry in high-grade rocks—case studies from the central Damara orogen (Namibia) and implications for the interpretation of Sm-Nd garnet ages and the role of high U-Th inclusions: Contributions to Mineralogy and Petrology, v. 146, p. 382-396.

Kirkland, C.L., Yakymchuk, C., Szilas, K., Evans, N., Hollis, J., McDonald, B. and Gardiner, N.J., 2018, Apatite: a U-Pb thermochronometer or geochronometer?: Lithos, v. 318, p. 143-157.

Landes, K.K., 1931, A paragenetic classification of the Magnet Cove minerals.: American Mineralogist: Journal of Earth and Planetary Materials, v. 16, no. 8, p. 313–326.

Metzger, F.W., Kelly, W.C., Nesbitt, B.E., and Essene, E.J., 1977, Scanning electron microscopy of daughter minerals in fluid inclusions: Economic Geology, v. 72, no. 2, p. 141–152, doi: 10.2113/gsecongeo.72.2.141.

Meyer, H.O., 1976, Kimberlites of the Continental United States: A Review: The Journal of Geology, v. 84, no. 4, p. 377–403, doi: 10.1086/628206.

Millonig, L., Zeh, A., Gerdes, A. and Klemd, R., 2008, Neoarchaean high-grade metamorphism in the Central Zone of the Limpopo Belt (South Africa): Combined petrological and geochronological evidence from the Bulai pluton: Lithos, vol. 103, no. 3-4, p. 333-351.

Milton, C., Ingram, B.L., and Blade, L.V., 1961, Kimzeyite, a zirconium garnet from Magnet Cove, Arkansas.: American Mineralogist: Journal of Earth and Planetary Materials, v. 46, no. 5-6, p. 533–548.

Miser, H.D., 1929, Structure of the Ouachita Mountains of Oklahoma and Arkansas: Oklahoma Geological Survey, no. 50.

Miser, H.D., and Stevens, R.E., 1938, Taeniolite from Magnet Cove, Arkansas: American Mineralogist: Journal of Earth and Planetary Materials, v. 23.2, p. 104–110.

Morgan, W. J., 1983, Hotspot tracks and the early rifting of the Atlantic: Tectonophysics v. 94, p. 123–139.

Nebel, O., Scherer, E.E. and Mezger, K., 2011, Evaluation of the 87Rb decay constant by age comparison against the U–Pb system: Earth and Planetary Science Letters, vol. 301, no. 1-2, p. 1-8.

Nesbitt, B.E., and Kelly, W.C., 1977, Magmatic and hydrothermal inclusions in carbonatite of the Magnet Cove Complex, Arkansas: Contributions to Mineralogy and Petrology, v. 63, no. 3, p. 271–294, doi: 10.1007/bf00375576.

Pidgeon, R.T., Bosch, D. and Bruguier, O., 1996, Inherited zircon and titanite U-Pb systems in an Archaean syenite from southwestern Australia: implications for U-Pb stability of titanite: Earth and Planetary Science Letters, v. 141, no. 1-4, p. 187-198.

Scharon, L. and Hsu, I.C., 1969, Paleomagnetic investigation of some Arkansas alkalic igneous rocks: Journal of Geophysical Research, vol. 74, no. 10, p. 2774-2779.

Scott, D.J. and St-Onge, M.R., 1995, Constraints on Pb closure temperature in titanite based on rocks from the Ungava orogen, Canada: Implications for U-Pb geochronology and PTt path determinations: Geology, v. 23, no. 12, p. 1123-1126.

Thomas, W. A. 2006, Tectonic inheritance at a continental margin: GSA Today, vol. 16, 4–11

Vogt, P. R., and Jung, W.-Y. 2007, Origin of the Bermuda volcanoes and Bermuda Rise: history, observations, models, and puzzles. *In* Foulger, G. R., and Jurdy, D. M., eds. Plates, plumes and planetary processes: Geol. Soc. Am. Spec. Pap., v. 430, p. 553–591.

Washington, H.S., 1900, Igneous complex of Magnet Cove, Arkansas: Geological Society of America Bulletin, v. 11, no. 1, p. 389–416, doi: 10.1130/gsab-11-389.

Williams, Howel, 1941, Calderas and their origin: California Univ. Dept. Geol. Sci. Bull., v. 25, no. 6, p. 239-346.

Yang, Y.-H., Wu, F.-Y., Yang, J.-H., Mitchell, R.H., Zhao, Z.-F., Xie, L.-W., Huang, C., Ma, Q., Yang, M., and Zhao, H., 2018, U–Pb age determination of schorlomite garnet by laser ablation inductively coupled plasma mass spectrometry: Journal of Analytical Atomic Spectrometry, v. 33, no. 2, p. 231–239, doi: 10.1039/c7ja00315c.

Zartman, R.E., 1977, Geochronology of some alkalic rock provinces in Eastern and Central United States: Annual Review of Earth and Planetary Sciences, v. 5, no. 1, p. 257–286, doi: 10.1146/annurev.ea.05.050177.001353.

Zartman, R.E., and Howard, J.M., 1987, Uranium-lead age of large zircon crystals from the potash sulfur Springs Igneous Complex, Garland County, Arkansas: Geological Society of America Special Papers, p. 235–240, doi: 10.1130/spe215-p235.

Zartman, R.E., Brock, M.R., Heyl, A.V., and Thomas, H.H., 1967, K-Ar and Rb-Sr ages of some alkalic intrusive rocks from central and eastern United States: American Journal of Science, v. 265, no. 10, p. 848–870, doi: 10.2475/ajs.265.10.848.

Appendix A: U-Pb Perovskite Data

Table 3: LA-ICP-MS U-Th-Pb Data for reference material IR6

Data for IsoplotR TW Plot						Element Concentrations					
Spot #	238U/206Pb	2SE	07Pb/206Pb	2SE	Error Correl.	U (ppm)	2SE (ppm)	Th (ppm)	2SE (ppm)	Pb (ppm)	2SE (ppm)
P_IR6_1	0.4255	0.017	0.05659	0.0017	0.51285	135.3	6	2442	90	49.9	1.4
P_IR6_2	0.4355	0.018	0.05724	0.0017	0.17903	141.5	5.6	2568	64	54	1.5
P_IR6_3	0.419	0.017	0.0573	0.0017	0.5573	128.2	5.9	2090	84	43.7	1.5
P_IR6_4	0.4281	0.016	0.05722	0.0017	0.45088	132.2	6	2208	74	46	1.7
P_IR6_5	0.4397	0.017	0.0582	0.0017	0.61793	125.4	5.7	2204	72	47.9	1.5
P_IR6_6	0.4378	0.017	0.05911	0.0017	0.40292	125	5.5	2403	77	51.3	1.7
P_IR6_7	0.4315	0.017	0.05882	0.0017	0.32542	125.6	5.7	2333	72	49.6	1.7
P_IR6_8	0.4399	0.017	0.05842	0.0017	0.052015	106.9	4	1716	63	35.4	1
P_IR6_9	0.4147	0.016	0.05716	0.0017	0.5391	128.7	6.2	2019	74	41.5	1.3
P_IR6_10	0.4271	0.016	0.05687	0.0016	0.56138	126.1	5.7	2213	68	45.3	1.4
P_IR6_11	0.4358	0.017	0.05853	0.0017	0.4386	122.3	5	2251	73	48.2	1.4
P_IR6_12	0.4253	0.016	0.05766	0.0017	0.35637	123.3	5.9	1948	67	40.4	1.3
P_IR6_13	0.4099	0.016	0.05652	0.0016	0.51552	130.6	6.1	2012	62	42.6	1.3
P_IR6_14	0.4313	0.017	0.05869	0.0017	0.38689	122	5.2	2012	66	44.1	1.6
P_IR6_15	0.4337	0.017	0.05912	0.0017	0.42292	125.5	5.6	1981	61	43.1	1.5
P_IR6_16	0.4296	0.017	0.05775	0.0016	0.27302	119.7	5.2	1977	73	40.4	1.2
P_IR6_17	0.4331	0.017	0.05767	0.0018	0.41862	127.1	6	2072	73	42.8	1.4
P_IR6_18	0.4397	0.018	0.05762	0.0016	0.39564	128.1	5.7	2103	71	42.5	1.4
P_IR6_19	0.4254	0.017	0.05667	0.0016	0.54623	122.4	5.4	2224	82	43	1.6
P_IR6_20	0.4207	0.017	0.05686	0.0016	0.47081	118.9	5.8	2106	73	40.5	1.2
P_IR6_21	0.4303	0.017	0.05754	0.0017	0.19501	125.8	5.4	2226	73	45.9	1.5
P_IR6_22	0.4349	0.017	0.05718	0.0016	0.25412	128.2	5.9	2167	70	45.1	1.3
P_IR6_23	0.4267	0.017	0.05749	0.0017	0.31332	124.1	5.6	2212	79	45.3	1.4
P_IR6_24	0.4316	0.017	0.05876	0.0017	0.42554	129.2	6.1	2244	69	47.8	1.5
P_IR6_25	0.4262	0.017	0.05798	0.0017	0.34316	129.1	6	2232	76	48.1	1.7
P_IR6_26	0.4332	0.016	0.05794	0.0017	0.4078	128.5	5.6	2287	70	48.2	1.6

Table 4: LA-ICP-MS U-Th-Pb Data for reference material Afr

Data for IsoplotR TW Plot						Element Concentrations					
Spot #	238U/206Pb	2SE	207Pb/206Pb	2SE	Error Correl.	U (ppm)	2SE (ppm)	Th (ppm)	2SE (ppm)	Pb (ppm)	2SE (ppm)
Afr30_1	1.081	0.041	0.0695	0.0019	0.54865	206.8	7.2	4760	140	95.8	1.8
Afr30_2	1.092	0.042	0.06847	0.002	0.52057	202.8	8.8	4800	180	95.8	2.9
Afr30_3	1.11	0.042	0.06998	0.002	0.51722	197.1	7.9	4570	160	92	2
Afr30_4	1.107	0.042	0.0704	0.002	0.5978	192.1	8.2	4110	150	83	1.9
Afr30_5	1.087	0.041	0.06866	0.0019	0.45359	199.6	9.9	4530	180	89.8	2.8
Afr30_6	1.168	0.054	0.07127	0.0021	0.83252	202	10	5370	230	106.8	3.3
Afr30_7	1.104	0.041	0.0704	0.002	0.44925	206.8	9.2	5160	210	104.4	2.9
Afr30_8	1.117	0.041	0.0705	0.0019	0.62348	205.5	9.1	4950	200	98.7	2.6
Afr30_9	1.109	0.043	0.07098	0.002	0.60366	200.7	9.8	4540	190	92.5	2.9
Afr30_10	1.11	0.042	0.07077	0.002	0.468	195.2	9.5	4170	180	83.9	2.3
Afr30_11	1.115	0.042	0.07059	0.002	0.49016	195.7	9.1	4230	170	85.2	2.4
Afr30_12	1.123	0.043	0.07088	0.002	0.6056	198.6	9.6	4160	170	85.1	2.3
Afr30_13	1.311	0.051	0.07374	0.0021	0.68869	173.4	8.4	3980	170	81.3	2.2
Afr30_14	1.209	0.046	0.07238	0.002	0.49866	197.6	8.7	6250	210	122.2	2.9
Afr30_15	1.338	0.05	0.07356	0.0021	0.52427	179.4	8.8	4910	210	96.1	2.8
Afr30_16	1.32	0.051	0.07483	0.0021	0.50808	175.5	8.6	4410	100	90.5	1.7
Afr30_17	1.238	0.054	0.07213	0.0021	0.74388	231	14	7550	340	138.3	6.1
Afr30_18	1.09	0.043	0.07015	0.002	0.48692	239	11	7440	290	142.3	4.3
Afr30_19	1.081	0.04	0.06929	0.0019	0.58168	238	11	7160	290	138	4.4
Afr30_20	1.078	0.039	0.06892	0.0019	0.44098	238	12	7100	290	136.5	4.3
Afr30_21	1.206	0.062	0.07049	0.0021	0.78666	245	12	7690	310	147.3	4.2
Afr30_22	1.091	0.041	0.06893	0.0019	0.55689	240	13	7830	350	147.5	4.8
Afr30_23	1.095	0.041	0.06896	0.0019	0.56541	239	13	7590	360	144.7	4.9
Afr30_24	1.101	0.04	0.06919	0.0019	0.45797	244	12	8440	370	161.6	5.2
Afr30_25	1.102	0.041	0.06945	0.0019	0.31107	249	13	9420	390	176.3	5.5
Afr30_26	1.087	0.041	0.06856	0.0019	0.60249	240	12	7770	280	147.4	3.7
Afr30_27	1.073	0.04	0.06831	0.0019	0.54763	234	12	4920	230	98.5	3.4
Afr30_28	1.075	0.04	0.06884	0.0019	0.74553	234	12	5630	240	109.1	3.2
Afr30_29	1.079	0.039	0.06907	0.0019	0.65569	221	11	5770	250	113.1	3.5
Afr30_30	1.089	0.041	0.06937	0.0019	0.24619	222	11	5400	210	107.5	3.2
Afr30_31	1.101	0.042	0.06957	0.0019	0.46822	233	11	7180	220	138.3	3.1
Afr30_32	1.089	0.041	0.06888	0.0019	0.51033	235	12	8480	340	161.9	5.5
Afr30_33	1.094	0.039	0.06921	0.0019	0.49296	237	12	8720	380	166.2	5.4
Afr30_34	1.131	0.043	0.07133	0.002	0.45141	208	8.8	5760	210	118	3.3
Afr30_35	1.127	0.044	0.07142	0.002	0.55752	206.8	9	5220	190	107.3	3
Afr30_36	1.133	0.044	0.07155	0.002	0.61179	206.6	9.4	5470	210	112.1	3.1

Table 5: LA-ICP-MS U-Th-Pb Data for reference material EAfr

Data for IsoplotR TW Plot						Element Concentrations					
Spot #	238U/206Pb	2SE	207Pb/206Pb	2SE	Error Correl.	U (ppm)	2SE (ppm)	Th (ppm)	2SE (ppm)	Pb (ppm)	2SE (ppm)
EAfr_1	1.171	0.042	0.06893	0.0019	0.7077	243	13	5370	230	96.9	2.6
EAfr_2	1.205	0.045	0.07056	0.0021	0.865	246	12	5540	240	99	2.8
EAfr_3	1.209	0.044	0.07004	0.002	0.739	239	13	5490	220	98.5	2.5
EAfr_4	1.21	0.044	0.07099	0.0019	0.7247	237	12	5600	250	100.8	3.1
EAfr_5	1.218	0.044	0.07085	0.002	0.7167	235	13	5390	320	97.6	3.6
EAfr_6	1.192	0.043	0.0705	0.002	0.7819	239	13	5480	300	101.3	3.6
EAfr_7	1.185	0.043	0.07034	0.002	0.722	245	13	5630	280	102.1	3.3
EAfr_8	1.189	0.043	0.07026	0.0019	0.5235	241	12	5630	270	102	3.3
EAfr_9	1.21	0.044	0.07136	0.002	0.7912	234	13	5590	330	103.8	4.2
EAfr_10	1.201	0.044	0.07043	0.0019	0.695	235	13	5580	290	101.5	3.3
EAfr_11	1.184	0.043	0.0707	0.0019	0.7808	238	13	5440	280	100.2	3.4
EAfr_12	1.198	0.043	0.07123	0.0019	0.6717	233	12	5430	270	100.2	3.3
EAfr_13	1.254	0.046	0.07128	0.002	0.6087	229	11	5420	230	103.1	2.7
EAfr_14	1.252	0.045	0.07151	0.002	0.6545	238	12	5770	250	108	3
EAfr_15	1.209	0.044	0.07058	0.0019	0.7342	228	11	5550	250	98.1	2.7
EAfr_16	1.217	0.044	0.07039	0.0019	0.6386	226	12	5520	290	100	3.4
EAfr_17	1.232	0.044	0.07108	0.0019	0.6281	226	11	5950	360	105.8	4.2
EAfr_18	1.247	0.045	0.07181	0.002	0.8079	227	12	6230	280	110.8	3.1
EAfr_19	1.224	0.044	0.07031	0.0019	0.6374	228	11	6230	230	110.7	2.3
EAfr_20	1.221	0.044	0.07076	0.002	0.741	230	12	5950	270	109.1	3
EAfr_21	1.211	0.044	0.07012	0.0019	0.7166	227	10	6180	270	107.8	2.9
EAfr_22	1.191	0.043	0.06969	0.0019	0.7833	226	11	6000	220	106.9	2.1
EAfr_23	1.218	0.045	0.07001	0.0019	0.4045	201.8	7.4	4700	81	85.3	1.1
EAfr_24	1.213	0.045	0.07028	0.0019	0.4988	203.4	6.8	4714	70	87.2	1.1
EAfr_25	1.208	0.044	0.07057	0.0019	0.638	217	10	5640	290	101.5	3
EAfr_26	1.221	0.044	0.07094	0.0019	0.7744	225	12	5670	260	105.5	3.1
EAfr_27	1.219	0.044	0.07109	0.0019	0.6595	215	11	5790	240	107.3	3
EAfr_28	1.218	0.044	0.0709	0.002	0.7057	229	11	6220	290	112.8	3.7
EAfr_29	1.215	0.044	0.07055	0.002	0.5735	238	12	6410	360	115.1	4.2
EAfr_30	1.228	0.046	0.07087	0.002	0.6357	235	12	6220	290	113.7	3.1
EAfr_31	1.244	0.045	0.07104	0.002	0.7286	241	11	6500	220	121.5	2.7

Table 6: LA-ICP-MS U-Th-Pb Data for sample MCper

Data for IsoplotR TW Plot						Element Concentrations					
Spot #	238U/206Pb	2SE	207Pb/206Pb	2SE	Error Correl.	U (ppm)	2SE (ppm)	Th (ppm)	2SE (ppm)	Pb (ppm)	2SE (ppm)
MCPer_1	0.3894	0.015	0.01895	0.00055	0.54411	256	10	10.65	0.39	4.51	0.14
MCPer_2	0.3893	0.015	0.0189	0.00055	0.53837	250	11	7.22	0.34	4.35	0.16
MCPer_3	0.3816	0.014	0.01884	0.00054	0.48526	249	12	8.39	0.37	4.39	0.15
MCPer_4	0.3826	0.014	0.01882	0.00055	0.70864	223.8	9.6	8.08	0.4	4.08	0.16
MCPer_5	0.354	0.013	0.01826	0.00051	0.47205	225	10	11.36	0.25	3.72	0.14
MCPer_6	0.3001	0.012	0.01735	0.0005	0.58568	257	12	10.67	0.39	3.41	0.13
MCPer_7	0.3043	0.012	0.01743	0.00051	0.51937	228.6	7.9	11.73	0.39	3.4	0.15
MCPer_8	0.3424	0.013	0.01801	0.00052	0.55526	237	12	10.16	0.39	3.83	0.2
MCPer_9	0.331	0.012	0.01777	0.0005	0.25853	234	11	9.54	0.41	3.67	0.16
MCPer_10	0.325	0.013	0.01786	0.00052	0.59332	236	11	9.46	0.31	3.58	0.15
MCPer_11	0.3367	0.014	0.01803	0.00052	0.53329	233	11	26.1	0.91	3.84	0.18
MCPer_12	0.3266	0.014	0.01778	0.00051	0.4801	238	12	27	1.3	3.69	0.15
MCPer_13	0.334	0.013	0.01787	0.00051	0.4876	233	11	12.81	0.51	3.66	0.14
MCPer_14	0.3568	0.014	0.01845	0.00054	0.51723	215	11	11.92	0.41	3.76	0.15
MCPer_15	0.3174	0.013	0.01738	0.00051	0.27994	251	11	13.02	0.42	3.82	0.15
MCPer_16	0.3104	0.013	0.01747	0.00053	0.69455	220.2	9.8	18.36	0.42	3.34	0.13
MCPer_17	0.3266	0.013	0.01784	0.00051	0.4637	238	11	13.69	0.25	3.78	0.14
MCPer_18	0.3404	0.014	0.01807	0.00056	0.48312	231	11	11.38	0.44	3.91	0.15
MCPer_19	0.3047	0.014	0.01726	0.00054	0.72392	221.4	7.8	15.4	1.1	3.39	0.13
MCPer_20	0.3254	0.013	0.0177	0.00052	0.46868	224	9.8	15.8	1	3.55	0.13
MCPer_21	0.341	0.02	0.01837	0.00059	0.28889	270.6	3.8	18.7	1.1	3.99	0.2
MCPer_22	0.3336	0.013	0.01785	0.00052	0.49368	229	11	30.1	1.3	3.92	0.18
MCPer_23	0.3056	0.012	0.01734	0.00049	0.4302	238	11	16	0.64	3.69	0.15
MCPer_24	0.3041	0.012	0.01751	0.0005	0.54201	246	12	15.66	0.67	3.89	0.14
MCPer_25	0.2989	0.012	0.01741	0.0005	0.32249	247	12	13.6	0.56	3.75	0.15
MCPer_26	0.3011	0.012	0.01729	0.0005	0.39755	255	14	14.28	0.56	3.96	0.15
MCPer_27	0.3231	0.014	0.01762	0.00057	0.37288	244	19	14.4	1	4.02	0.22
MCPer_28	0.3062	0.013	0.01734	0.00049	0.4687	248	14	14.04	0.69	3.86	0.15
MCPer_29	0.3194	0.014	0.01828	0.00054	0.15351	289	13	15.42	0.49	4.79	0.16
MCPer_30	0.349	0.016	0.01829	0.00058	0.41225	197.9	7.5	12.91	0.5	3.9	0.14
MCPer_31	0.319	0.017	0.01768	0.00061	0.48048	215.5	5.9	12.02	0.64	3.86	0.17
					averages:	U (ppm)		Th (ppm)		Pb (ppm)	
						13.66		14.19		3.85	

Appendix B: U-Pb Ti-Garnet Data Session

Table 7: LA-ICP-MS U-Th-Pb Data for reference material Mali

Data for IsoplotR TW Plot						Element Concentrations					
Spot #	238U/206Pb	2SE	207Pb/206Pb	2SE	Error Correl.	U (ppm)	2SE (ppm)	Th (ppm)	2SE (ppm)	Pb (ppm)	2SE (ppm)
Mali_1	29.42908	0.8487	0.0578	0.0025	0.29755	4.87	0.39	0.603	0.027	0.0155	0.003
Mali_2	28.57143	0.898	0.063	0.0017	0.48477	8.1	0.29	0.701	0.049	0.024	0.0019
Mali_3	28.81844	1.1627	0.0512	0.0023	0.32594	4.266	0.09	0.792	0.018	0.0126	0.0011
Mali_4	29.30832	0.9449	0.0504	0.0014	0.17759	4.859	0.088	0.956	0.019	0.01598	0.00097
Mali_5	29.81515	0.9778	0.0643	0.0098	0.65792	3.41	0.064	0.712	0.012	0.0169	0.0051
Mali_6	29.46376	0.8073	0.0738	0.0039	0.45619	3.732	0.053	0.721	0.012	0.0218	0.0016
Mali_7	29.39447	0.864	0.052	0.0018	0.03565	3.661	0.042	0.7131	0.0092	0.01128	0.00099
Mali_8	29.35995	0.862	0.0522	0.0014	0.24803	3.658	0.061	0.711	0.016	0.01058	0.00071
Mali_9	28.66151	0.8215	0.0709	0.0031	-0.216	3.243	0.054	0.638	0.012	0.0182	0.0015
Mali_10	29.19708	0.9377	0.0558	0.0022	0.37599	3.824	0.067	0.782	0.017	0.0116	0.0011
Mali_11	26.96872	0.8728	0.114	0.0033	0.19429	3.065	0.06	0.673	0.016	0.0372	0.0021
Mali_12	29.10361	0.9317	0.0541	0.0026	0.11692	4.379	0.073	0.873	0.018	0.0147	0.0022
Mali_13	29.24832	0.941	0.052	0.0018	0.43076	3.334	0.056	0.681	0.014	0.01023	0.00095
Mali_14	29.36858	0.9488	0.058	0.0032	-0.019567	3.27	0.046	0.6177	0.0091	0.012	0.001
Mali_15	28.71913	0.8083	0.0583	0.0021	0.031316	3.286	0.037	0.614	0.012	0.0129	0.0011
Mali_16	28.32059	0.8021	0.0521	0.0017	0.27913	3.394	0.061	0.665	0.015	0.0117	0.0012
Mali_17	29.35995	0.9482	0.0515	0.0018	0.048768	3.329	0.057	0.668	0.014	0.01066	0.00087
Mali_18	29.77077	0.842	0.0567	0.0046	-0.037534	3.273	0.058	0.597	0.012	0.01011	0.00089
Mali_19	29.49853	1.1312	0.0507	0.002	-0.002673	3.109	0.056	0.643	0.011	0.0095	0.0011
Mali_20	27.3224	0.8958	0.101	0.011	-0.41241	3.159	0.056	0.67	0.018	0.0316	0.0061
Mali_21	29.35995	0.862	0.0528	0.0022	0.41765	2.802	0.041	0.559	0.011	0.00846	0.00079
Mali_22	28.97711	0.8145	0.0533	0.0023	0.23852	2.957	0.038	0.566	0.011	0.00924	0.00096
Mali_23	29.41176	0.8651	0.0643	0.0089	0.23123	3.333	0.047	0.653	0.011	0.0162	0.0037
Mali_24	29.86858	0.8921	0.0535	0.002	0.6737	3.548	0.054	0.675	0.015	0.0117	0.00092
Mali_25	28.66151	0.8215	0.0539	0.0021	0.19429	3.329	0.055	0.634	0.014	0.0108	0.0011
Mali_26	29.08668	0.846	0.0512	0.0019	0.46444	3.176	0.051	0.628	0.011	0.0106	0.001

Table 8: LA-ICP-MS U-Th-Pb Data for sample LJ

Data for IsoplotR TW Plot						Element Concentrations					
Spot #	238U/206Pb	2SE	207Pb/206Pb	2SE	Error Correl.	U (ppm)	2SE (ppm)	Th (ppm)	2SE (ppm)	Pb (ppm)	2SE (ppm)
LJ_1	150.3759	8.3668	0.114	0.019	0.23553	0.684	0.011	4.94	0.11	0.0139	0.001
LJ_2	163.3987	8.2767	0.1	0.019	0.0937	0.705	0.014	4.923	0.096	0.0144	0.001
LJ_3	131.5789	6.2327	0.209	0.029	-0.11986	0.672	0.011	4.759	0.091	0.0152	0.0011
LJ_4	93.37068	6.9745	0.416	0.039	0.088053	0.606	0.011	4.691	0.089	0.0222	0.002
LJ_5	160.7717	8.5297	0.103	0.058	0.055514	0.6118	0.0099	4.723	0.07	0.0123	0.0011
LJ_6	123.4568	6.5539	0.258	0.026	-0.12067	0.6504	0.0091	4.936	0.068	0.0173	0.0013
LJ_7	166.9449	8.9186	0.093	0.014	0.13745	0.677	0.01	5.072	0.073	0.0153	0.00095
LJ_8	150.3759	9.7236	0.131	0.035	-0.1098	0.716	0.015	5.21	0.1	0.0137	0.0014
LJ_9	161.8123	8.3786	0.073	0.014	-0.22982	0.717	0.012	5.114	0.09	0.0128	0.0012
LJ_10	49.43154	2.4435	0.606	0.028	0.23238	0.706	0.011	5.279	0.095	0.0469	0.0027
LJ_11	94.33962	5.874	0.453	0.094	-0.18805	0.716	0.016	5.1	0.15	0.0223	0.0016
LJ_12	163.9344	8.0623	0.114	0.046	-0.10179	0.6934	0.0097	4.661	0.079	0.014	0.00082
LJ_13	125.9446	8.7241	0.271	0.03	0.21998	0.645	0.01	4.332	0.076	0.0165	0.0016
LJ_14	164.7446	9.2279	0.086	0.019	0.062518	0.609	0.01	4.195	0.059	0.0115	0.00094
LJ_15	102.9866	4.3486	0.369	0.018	0.13551	0.5696	0.0087	4.063	0.073	0.0168	0.0014
LJ_16	168.3502	9.3528	0.089	0.031	0.040333	0.5537	0.007	4.098	0.079	0.0103	0.001
LJ_17	151.2859	7.0951	0.117	0.02	0.09079	0.5923	0.0071	4.515	0.085	0.0126	0.001
LJ_18	153.1394	7.739	0.065	0.013	0.017972	0.5757	0.0069	4.284	0.08	0.0108	0.00088
LJ_19	159.2357	8.8746	0.111	0.023	-0.14795	0.6132	0.0081	4.397	0.069	0.0126	0.0015
LJ_20	155.2795	8.6802	0.134	0.02	0.1392	0.6387	0.0085	4.624	0.078	0.0131	0.00094
LJ_21	154.7988	8.3869	0.181	0.038	0.52746	0.686	0.011	4.644	0.064	0.02	0.01
LJ_22	153.8462	8.9941	0.164	0.059	-0.05709	0.7152	0.0089	4.979	0.068	0.0163	0.0011
LJ_23	119.3317	8.9712	0.315	0.034	-0.02332	0.714	0.011	4.746	0.071	0.0193	0.0022
LJ_24	144.0922	10.589	0.324	0.062	0.044075	0.7079	0.0099	4.998	0.081	0.0171	0.0022
LJ_25	81.76615	5.0143	0.397	0.037	0.48881	0.722	0.015	4.879	0.059	0.0255	0.0028
LJ_26	137.741	6.4507	0.189	0.017	0.31367	0.7223	0.0099	4.756	0.054	0.018	0.0013

Table 9: LA-ICP-MS U-Th-Pb Data for sample MC-5

Data for IsoplotR TW Plot						Element Concentrations					
Spot #	238U/206Pb	2SE	207Pb/206Pb	2SE	Error Correl.	U (ppm)	2SE (ppm)	Th (ppm)	2SE (ppm)	Pb (ppm)	2SE (ppm)
MC5_1	57.67013	1.8625	0.0979	0.0034	0.10973	4.316	0.058	0.651	0.021	0.0224	0.0017
MC5_2	56.11672	1.606	0.0947	0.0032	0.25722	4.661	0.064	0.4441	0.0087	0.0202	0.0013
MC5_3	55.67929	1.9221	0.1059	0.0049	-0.15713	4.492	0.063	0.587	0.012	0.0233	0.0012
MC5_4	54.64481	1.8812	0.1067	0.0048	0.20195	4.785	0.079	0.621	0.015	0.028	0.0025
MC5_5	52.9661	2.2443	0.124	0.016	-0.66722	5.47	0.13	3.03	0.11	0.061	0.011
MC5_6	53.3049	2.3015	0.12	0.01	-0.80465	4.328	0.05	0.522	0.011	0.0342	0.0097
MC5_7	56.5931	1.7936	0.1027	0.0039	0.20849	4.481	0.053	0.6608	0.0098	0.0238	0.0017
MC5_8	56.02241	1.7576	0.1006	0.0034	0.19843	3.9	0.045	0.547	0.011	0.0192	0.0012
MC5_9	58.41121	1.6377	0.0917	0.0029	0.38784	5.121	0.056	1.97	0.03	0.0313	0.0018
MC5_10	56.14823	1.5763	0.1008	0.0043	0.24359	4.322	0.046	0.55	0.016	0.0225	0.0017
MC5_11	55.83473	1.5899	0.0999	0.0039	-0.21346	4.241	0.045	0.553	0.014	0.0224	0.0013
MC5_12	56.94761	1.6215	0.0969	0.0062	0.29339	4.661	0.055	1.714	0.042	0.0262	0.0023
MC5_13	55.61735	1.7941	0.1033	0.0067	-0.50582	4.155	0.055	0.629	0.014	0.0226	0.002
MC5_14	55.34034	1.6538	0.0902	0.0026	0.49523	4.469	0.05	0.878	0.028	0.0239	0.0013
MC5_15	54.76451	1.4996	0.0991	0.0027	0.18957	4.264	0.052	0.847	0.023	0.0232	0.0013
MC5_16	56.85048	1.7129	0.1064	0.0039	0.021661	4.572	0.046	0.855	0.078	0.0266	0.0022
MC5_17	56.27462	1.7418	0.0903	0.0029	0.26999	4.947	0.06	1.041	0.028	0.0268	0.0016
MC5_18	55.99104	2.1004	0.0947	0.0059	-0.33466	4.626	0.049	0.856	0.014	0.0258	0.0028
MC5_19	54.46623	1.6909	0.1051	0.0068	-0.32098	4.282	0.04	1.031	0.019	0.0281	0.0026
MC5_20	54.67469	2.6904	0.109	0.013	-0.74545	5.599	0.074	3.265	0.087	0.0605	0.0084
MC5_21	55.12679	1.9449	0.0968	0.0029	0.092353	4.146	0.059	0.777	0.025	0.0219	0.0012
MC5_22	57.50431	1.6534	0.0939	0.0033	0.051094	4.439	0.04	0.3908	0.0097	0.0184	0.0015
MC5_23	56.30631	1.6803	0.0962	0.0035	0.33857	4.735	0.05	1.543	0.04	0.0291	0.0016
MC5_24	55.77245	1.6797	0.1005	0.0037	0.034285	4.642	0.046	0.8	0.014	0.0259	0.0016
MC5_25	50	3.25	0.152	0.024	-0.63873	4.003	0.053	0.588	0.016	0.05	0.016
MC5_26	57.30659	1.6092	0.0989	0.0033	0.42613	4.192	0.056	0.4268	0.0097	0.0195	0.0014
MC5_27	56.43341	1.4968	0.0894	0.0034	0.28887	4.518	0.051	0.659	0.012	0.0203	0.0012
MC5_28	58.44535	1.7079	0.0862	0.0044	-0.08879	6.57	0.12	5.453	0.065	0.0605	0.0034
MC5_29	56.33803	1.7774	0.1083	0.004	-0.037402	4.238	0.056	0.4961	0.0077	0.0224	0.0013
MC5_30	56.9152	1.6845	0.1	0.0037	0.38614	3.867	0.041	0.2616	0.006	0.0168	0.0013
MC5_31	59.27682	2.0731	0.1053	0.0065	-0.089496	4.333	0.072	0.486	0.015	0.0204	0.002
MC5_32	48.6618	1.6339	0.2013	0.0099	0.39316	4.6	0.076	1.889	0.037	0.0781	0.0066
MC5_33	55.71031	1.8932	0.0995	0.0039	-0.24104	4.114	0.044	0.4323	0.0088	0.0233	0.0019
MC5_34	55.55556	3.7037	0.149	0.023	-0.8783	4.784	0.087	2.39	0.12	0.055	0.011
MC5_35	58.10575	1.5193	0.0928	0.0024	0.49665	4.356	0.039	0.3533	0.0068	0.0182	0.0011
MC5_36	58.30904	1.904	0.0934	0.009	-0.37889	5.596	0.061	4.773	0.084	0.0529	0.0049
MC5_37	56.46527	1.8173	0.0955	0.0083	-0.61897	5.524	0.069	4.774	0.077	0.0596	0.0053
MC5_38	43.10345	5.2021	0.219	0.043	-0.89183	5.592	0.073	4.385	0.084	0.143	0.037
MC5_39	57.67013	1.6962	0.076	0.0026	-0.0945	6.291	0.07	6.65	0.083	0.0669	0.0027
MC5_40	57.63689	1.7939	0.0881	0.0043	0.022534	5.188	0.054	4.542	0.081	0.0497	0.002
MC5_41	56.56109	2.0155	0.1008	0.0081	-0.55339	5.395	0.066	4.856	0.058	0.0588	0.0044
					averages:	U (ppm)		Th (ppm)		Pb (ppm)	
						4.70		1.66		0.04	

Table 10: LA-ICP-MS U-Th-Pb Data for sample MC-7

Data for IsoplotR TW Plot						Element Concentrations					
Spot #	238U/206Pb	2SE	207Pb/206Pb	2SE	Error Correl.	U (ppm)	2SE (ppm)	Th (ppm)	2SE (ppm)	Pb (ppm)	2SE (ppm)
MC7_1	59.1716	1.7156	0.0552	0.0023	0.25472	5.339	0.06	0.0702	0.0035	0.00297	0.00049
MC7_2	58.96226	1.8773	0.0528	0.0021	0.052114	4.789	0.081	0.055	0.0021	0.00275	0.00057
MC7_3	59.06675	1.884	0.0539	0.0016	0.27699	5.548	0.071	0.0673	0.0026	0.00317	0.00037
MC7_4	59.73716	1.6772	0.0571	0.0029	0.35371	6.379	0.087	0.0736	0.0031	0.00466	0.00087
MC7_5	57.97101	1.882	0.0546	0.0019	0.12187	6.582	0.098	0.0781	0.0031	0.00451	0.00069
MC7_6	58.61665	1.7523	0.0548	0.0023	0.34404	6.389	0.086	0.0721	0.0035	0.0031	0.00051
MC7_7	63.61323	2.428	0.0632	0.0045	-0.057507	5.5	0.11	0.0883	0.0074	0.0054	0.0015
MC7_8	57.67013	1.8625	0.0581	0.0031	0.33868	2.39	0.045	0.0254	0.0017	0.0022	0.00052
MC7_9	58.65103	1.7888	0.0559	0.0018	0.29135	9.201	0.087	0.146	0.005	0.0077	0.0012
MC7_10	58.07201	1.8885	0.0567	0.002	0.11791	6.034	0.063	0.0727	0.0036	0.00596	0.00083
MC7_11	54.88474	2.7111	0.095	0.013	-0.78887	10.23	0.12	0.1516	0.0056	0.05	0.022
MC7_12	59.10165	1.7465	0.0517	0.0018	0.59527	9.57	0.13	0.142	0.0038	0.0041	0.00047
MC7_13	58.78895	1.7626	0.0531	0.0016	0.51645	9.34	0.13	0.1745	0.0053	0.00454	0.00055
MC7_14	58.34306	1.8381	0.0523	0.0017	0.064433	8.88	0.12	0.1032	0.0037	0.00438	0.00061
MC7_15	58.37712	1.738	0.0535	0.0015	-0.50022	10.81	0.13	0.1381	0.0039	0.00484	0.00073
MC7_16	59.24171	1.6144	0.0529	0.0017	0.39218	9.59	0.12	0.1484	0.0057	0.00455	0.00051
MC7_17	59.20663	1.8228	0.0532	0.0015	0.63305	10.77	0.1	0.1289	0.0039	0.00465	0.00055
MC7_18	60.13229	1.5548	0.0543	0.0016	0.38885	9.202	0.097	0.1642	0.0061	0.0053	0.001
MC7_19	59.24171	1.7197	0.0554	0.0017	0.24301	12.46	0.13	0.071	0.0027	0.00664	0.00091
MC7_20	57.80347	1.8043	0.0581	0.0028	-0.20246	14.04	0.17	0.0899	0.0033	0.0128	0.0028
MC7_21	58.92752	1.7015	0.0503	0.0035	0.02682	1.642	0.027	0.0183	0.0014	0.00072	0.00038
MC7_22	58.47953	2.0861	0.0533	0.0031	-0.093633	2.622	0.04	0.0309	0.0019	0.00142	0.00035
MC7_23	59.88024	2.0438	0.0531	0.0014	0.32703	9.4	0.16	0.1244	0.004	0.00499	0.0007
MC7_24	57.93743	1.7119	0.0532	0.0018	-0.52581	9.22	0.12	0.1895	0.0049	0.00516	0.0007
MC7_25	59.06675	1.7444	0.0536	0.0018	0.15776	7.192	0.091	0.1396	0.0039	0.00477	0.00049
MC7_26	59.41771	1.6946	0.0546	0.0033	0.33487	1.972	0.032	0.0242	0.002	0.00088	0.00043
MC7_27	57.7034	1.6315	0.0522	0.0028	0.045648	2.789	0.032	0.0351	0.0022	0.00192	0.00053
MC7_28	58.51375	1.575	0.0529	0.0017	0.057113	5.884	0.069	0.0696	0.0029	0.00327	0.0006
MC7_29	58.13953	1.7577	0.0536	0.0014	0.36232	12.82	0.17	0.1551	0.0044	0.00569	0.00068
MC7_30	58.85815	1.5936	0.0536	0.0016	0.3785	8.639	0.097	0.1456	0.0061	0.00487	0.00066
MC7_31	58.30904	1.462	0.0519	0.0017	-0.050607	9.67	0.12	0.1176	0.0045	0.00386	0.00064
MC7_32	58.96226	1.8773	0.0609	0.0025	0.15498	3.794	0.046	2.44	0.27	0.0245	0.0029
MC7_33	60.49607	2.0495	0.0531	0.0027	0.35499	2.112	0.048	1.332	0.03	0.01032	0.00073
MC7_34	59.63029	2.0979	0.0554	0.0033	0.45751	2.253	0.034	0.56	0.022	0.00495	0.00067
MC7_35	60.35003	1.9667	0.0681	0.0039	-0.028382	2.534	0.067	1.928	0.061	0.0162	0.001
MC7_36	58.37712	1.6358	0.0498	0.0012	0.1506	12.35	0.14	0.1134	0.0037	0.00347	0.00051
MC7_37	58.10575	1.6544	0.0571	0.0017	0.28808	8.92	0.12	0.0375	0.0021	0.00601	0.00068
MC7_38	58.71991	1.8964	0.0577	0.0028	-0.37463	3.498	0.063	0.075	0.0046	0.00321	0.00094
MC7_39	59.10165	1.7814	0.0511	0.0014	0.51091	11.47	0.15	0.0252	0.0021	0.00399	0.00063
MC7_40	58.82353	1.7647	0.0497	0.0011	0.48017	14.07	0.14	0.0551	0.003	0.00477	0.00086
MC7_41	57.67013	1.4966	0.0565	0.0017	0.2361	13.14	0.12	0.024	0.0019	0.0103	0.0015
MC7_42	56.98006	1.5909	0.0509	0.0013	-0.10186	19.5	0.18	0.0912	0.004	0.0077	0.0065
MC7_43	58.37712	1.8743	0.0536	0.0021	0.37479	4.528	0.042	0.0617	0.0024	0.00264	0.00057
MC7_44	59.73716	1.6772	0.0517	0.0018	0.32276	4.861	0.057	0.0676	0.0031	0.00285	0.00058
MC7_45	57.07763	3.2579	0.081	0.01	0.052123	0.433	0.029	0.0064	0.0011	0.00088	0.00038
					averages:	U (ppm)		Th (ppm)		Pb (ppm)	
						7.519022		0.22061111		0.00630133	

Table 11: LA-ICP-MS U-Th-Pb Data for sample MC-11

Data for IsoplotR TW Plot						Element Concentrations					
Spot #	238U/206Pb	2SE	207Pb/206Pb	2SE	Error Correl.	U (ppm)	2SE (ppm)	Th (ppm)	2SE (ppm)	Pb (ppm)	2SE (ppm)
MC11_1	57.93743	1.8126	0.085	0.0045	-0.3983	9.68	0.12	5.476	0.086	0.0692	0.0044
MC11_2	60.24096	1.9959	0.0624	0.0033	-0.28267	8.48	0.14	5.284	0.051	0.0506	0.003
MC11_3	60.45949	1.8642	0.0539	0.0015	0.34397	9.19	0.13	5.873	0.074	0.0501	0.0023
MC11_4	60.45949	1.7911	0.0671	0.0042	-0.35752	9.7	0.12	5.734	0.062	0.0579	0.0037
MC11_5	60.79027	1.8108	0.0561	0.002	-0.021521	9.54	0.15	5.557	0.091	0.0496	0.0028
MC11_6	61.05006	2.4226	0.0644	0.0059	-0.11622	10.11	0.18	5.69	0.14	0.0627	0.0068
MC11_7	48.07692	5.3162	0.273	0.052	-0.85229	4.795	0.086	2.17	0.079	0.131	0.039
MC11_8	2.645503	0.5809	0.752	0.064	0.6262	4.709	0.097	2.245	0.048	4.82	0.62
MC11_9	37.73585	3.9872	0.288	0.042	-0.85711	6.456	0.068	3.495	0.05	0.245	0.057
MC11_10	48.07692	3.6982	0.187	0.043	-0.85241	5.894	0.091	3.646	0.07	0.115	0.038
MC11_11	50	3	0.178	0.026	-0.81891	5.171	0.095	2.488	0.066	0.083	0.015
MC11_12	51.65289	2.3745	0.181	0.023	-0.81928	7.85	0.12	4.533	0.088	0.125	0.019
MC11_13	57.50431	1.6203	0.0805	0.0038	-0.033596	8.257	0.097	4.117	0.071	0.0525	0.0032
MC11_14	54.43658	1.6002	0.1198	0.0033	0.11351	6.414	0.057	2.993	0.049	0.0629	0.0026
MC11_15	60.16847	2.2808	0.0589	0.0029	0.060162	6.954	0.097	2.903	0.067	0.0299	0.002
MC11_16	41.98153	1.2161	0.257	0.01	0.11436	7.861	0.065	3.215	0.053	0.1947	0.009
MC11_17	60.09615	1.6613	0.0597	0.0028	-0.047345	6.192	0.068	2.471	0.025	0.0255	0.0021
MC11_18	60.02401	1.7654	0.0695	0.0019	-0.11133	8.9	0.12	3.144	0.043	0.0369	0.0019
MC11_19	60.53269	1.7955	0.0573	0.0016	0.32979	7.26	0.078	2.843	0.036	0.0238	0.0014
MC11_20	61.57635	1.7821	0.0566	0.0019	0.27375	7.94	0.11	3.061	0.047	0.0285	0.0018
MC11_21	59.34718	1.7963	0.0716	0.0037	-0.42795	6.014	0.065	3.224	0.07	0.0362	0.0027
MC11_22	42.55319	3.9837	0.254	0.036	-0.68553	5.806	0.093	3.159	0.047	0.162	0.036
MC11_23	57.7034	1.8979	0.078	0.0035	-0.39777	5.512	0.075	2.993	0.048	0.0357	0.0029
MC11_24	50.32713	1.773	0.147	0.014	-0.574	5.611	0.07	3.172	0.046	0.0752	0.0083
MC11_25	57.87037	1.6745	0.0846	0.0038	-0.32448	6.083	0.065	3.476	0.072	0.0422	0.0023
MC11_26	59.66587	1.7444	0.0579	0.0023	0.11737	5.496	0.059	3.067	0.032	0.0295	0.0012
MC11_27	61.95787	1.8042	0.0629	0.0023	0.031353	5.714	0.052	3.131	0.046	0.0294	0.0016
MC11_28	29.08668	1.0152	0.447	0.017	-0.27163	5.591	0.077	3.087	0.061	0.364	0.02
MC11_29	48.85198	1.8853	0.1934	0.0096	-0.72883	5.418	0.054	2.919	0.042	0.0939	0.0075
MC11_30	25.83979	0.8012	0.4832	0.01	0.32315	5.165	0.059	2.755	0.043	0.415	0.012
MC11_31	60.64281	2.0594	0.0588	0.0023	-0.093534	8.07	0.13	3.062	0.052	0.0288	0.0017
MC11_32	60.16847	1.8463	0.0569	0.0018	0.15367	8.76	0.11	3.316	0.049	0.0319	0.0018
MC11_33	59.52381	1.9487	0.0808	0.007	-0.48278	6.236	0.083	3.374	0.036	0.0412	0.004
MC11_34	61.27451	1.652	0.0593	0.0031	-0.0030617	6.15	0.096	3.301	0.032	0.03	0.0024
MC11_35	52.93806	1.9617	0.115	0.012	-0.53907	6.923	0.087	3.7	0.067	0.071	0.011
MC11_36	46.08295	1.5715	0.2321	0.0058	-0.33599	8.14	0.11	3.248	0.041	0.1679	0.0085
MC11_37	60.82725	2.109	0.072	0.0094	-0.67836	8.914	0.088	3.466	0.059	0.0426	0.0082
MC11_38	41.68404	1.1642	0.2734	0.0089	-0.196	7.711	0.08	3.211	0.05	0.214	0.012
MC11_39	60.93845	2.1167	0.0565	0.0022	0.13828	7.823	0.079	2.83	0.048	0.0287	0.0019
MC11_40	58.54801	1.6454	0.0592	0.002	0.31726	6.096	0.073	4.411	0.053	0.0409	0.0017
MC11_41	58.30904	1.598	0.0596	0.0019	0.42003	6.818	0.059	4.598	0.07	0.0444	0.002
MC11_42	58.71991	2.7584	0.108	0.019	-0.7512	6.465	0.093	3.951	0.093	0.063	0.012
MC11_43	58.68545	1.7909	0.0685	0.0025	0.51155	6.95	0.097	4.596	0.091	0.0494	0.0025
MC11_44	57.24098	1.4744	0.0685	0.0025	-0.055319	8.11	0.11	4.447	0.071	0.0486	0.0023
MC11_45	57.73672	1.6668	0.0635	0.0015	0.36441	9.49	0.12	4.75	0.065	0.0464	0.0022
					averages:	U (ppm)		Th (ppm)		Pb (ppm)	
						7.120422		3.64848889		0.18990444	

Table 12: LA-ICP-MS U-Th-Pb Data for sample MC-30

Data for IsoplotR TW Plot						Element Concentrations					
Spot #	238U/206Pb	2SE	207Pb/206Pb	2SE	Error Correl.	U (ppm)	2SE (ppm)	Th (ppm)	2SE (ppm)	Pb (ppm)	2SE (ppm)
MC30_1	50.50505	4.5914	0.119	0.027	-0.90014	5.588	0.081	0.871	0.023	0.064	0.032
MC30_2	37.45318	2.8055	0.307	0.033	-0.46969	3.425	0.066	0.615	0.016	0.104	0.017
MC30_3	49.95005	1.8463	0.175	0.021	-0.25059	2.225	0.069	0.247	0.012	0.0229	0.0046
MC30_4	45.26935	1.5575	0.19	0.014	-0.21799	3.755	0.06	0.376	0.014	0.0515	0.0058
MC30_5	28.57143	1.0612	0.389	0.011	0.064021	3.071	0.039	0.2799	0.0065	0.1627	0.0065
MC30_6	55.34034	2.1132	0.0755	0.008	-0.69832	3.12	0.05	0.2954	0.0098	0.0095	0.0027
MC30_7	55.4939	2.0633	0.0802	0.0074	-0.16263	2.185	0.036	0.2326	0.0056	0.0088	0.0018
MC30_8	55.89715	1.9059	0.064	0.0047	-0.05402	2.658	0.038	0.2772	0.0085	0.00634	0.00066
MC30_9	55.55556	1.6667	0.0619	0.0053	-0.16658	2.935	0.039	0.3009	0.0088	0.0068	0.0016
MC30_10	58.30904	1.972	0.0592	0.0036	0.095934	2.424	0.029	0.2557	0.0066	0.00399	0.00058
MC30_11	40.32258	4.2274	0.237	0.047	-0.87014	2.585	0.027	0.2697	0.0064	0.088	0.04
MC30_12	57.8369	1.8733	0.0616	0.0026	0.32762	2.657	0.024	0.3138	0.0074	0.00551	0.00065
MC30_13	58.41121	2.0471	0.0616	0.0053	0.72381	2.692	0.035	0.2575	0.0093	0.0056	0.0016
MC30_14	56.46527	1.6579	0.0607	0.0027	0.25332	2.591	0.034	0.2864	0.0078	0.00543	0.00072
MC30_15	57.63689	1.661	0.0585	0.0025	0.48044	2.611	0.034	0.2683	0.0079	0.00456	0.00067
MC30_16	56.75369	1.9004	0.0579	0.003	-0.29952	2.86	0.033	0.2788	0.0062	0.0053	0.00074
MC30_17	47.39336	5.1661	0.139	0.033	-0.89981	3.905	0.061	0.836	0.027	0.075	0.036
MC30_18	56.85048	1.7776	0.06	0.0044	-0.021376	3.293	0.045	0.3154	0.0081	0.00586	0.00074
MC30_19	55.77245	2.4885	0.075	0.01	-0.76822	5.56	0.076	0.885	0.014	0.0204	0.0069
MC30_20	54.52563	1.6352	0.0672	0.0052	0.069641	3.15	0.05	0.338	0.009	0.0081	0.0018
MC30_21	54.67469	1.7338	0.067	0.0067	-0.43002	2.774	0.048	0.2865	0.0081	0.0065	0.0015
MC30_22	56.27462	1.8684	0.0623	0.0031	0.17225	3.498	0.058	0.3793	0.0079	0.00704	0.00095
MC30_23	58.61665	1.8554	0.0608	0.0025	-0.10173	3.514	0.048	0.3524	0.0079	0.0071	0.0021
MC30_24	55.37099	1.8702	0.0655	0.0052	-0.52431	3.564	0.048	0.3667	0.0091	0.0091	0.0024
MC30_25	39.37008	6.665	0.186	0.048	-0.90848	3.173	0.045	0.3101	0.0071	0.087	0.04
MC30_26	57.5374	2.0856	0.0607	0.0041	0.31468	2.427	0.042	0.271	0.01	0.00558	0.00096
MC30_27	56.7215	1.7695	0.0626	0.0036	0.049469	2.083	0.028	0.2214	0.0048	0.00447	0.00076
MC30_28	54.97526	1.7529	0.0585	0.003	0.2534	2.235	0.029	0.2397	0.0084	0.00375	0.0008
MC30_29	56.98006	1.8182	0.0616	0.0039	0.33326	2.107	0.026	0.2103	0.0054	0.00407	0.00041
MC30_30	57.67013	1.7294	0.06	0.0029	0.2359	2.152	0.032	0.2139	0.0062	0.00358	0.00059
MC30_31	55.06608	1.9407	0.0851	0.0063	-0.39695	2.183	0.031	0.2354	0.0076	0.007	0.0014
MC30_32	57.07763	1.8244	0.0568	0.0029	0.38603	2.103	0.028	0.2263	0.0063	0.00418	0.00056
MC30_33	56.75369	2.1903	0.0634	0.0049	0.13954	3.979	0.077	0.497	0.014	0.0089	0.0015
MC30_34	57.43825	1.8145	0.0594	0.0021	0.33297	4.241	0.058	1.156	0.019	0.0141	0.00099
MC30_35	57.37235	1.58	0.0565	0.0018	0.41553	6.599	0.065	2.011	0.034	0.0209	0.0011
MC30_36	57.11022	1.5656	0.0623	0.0019	0.33155	7.086	0.077	1.258	0.023	0.0186	0.0013
MC30_37	55.61735	2.0106	0.0771	0.0085	-0.34081	6.589	0.082	1.196	0.02	0.0247	0.0045
MC30_38	56.78592	2.0638	0.073	0.0062	-0.4363	6.76	0.12	1.433	0.018	0.0254	0.0041
MC30_39	50.83884	1.8092	0.1605	0.0083	-0.07514	2.121	0.027	0.2145	0.005	0.0231	0.002
MC30_40	58.20722	1.5924	0.0604	0.0025	-0.16665	4.132	0.042	1.006	0.021	0.0135	0.0011
MC30_41	43.85965	5.3863	0.15	0.037	-0.90665	5.405	0.06	1.151	0.018	0.128	0.062
MC30_42	56.02241	2.2283	0.082	0.011	-0.55922	5.048	0.055	0.9	0.018	0.0213	0.0044
MC30_43	50.25126	2.3232	0.152	0.018	-0.64721	3.706	0.047	0.944	0.015	0.0433	0.0066
MC30_44	35.34818	1.162	0.3428	0.0093	-0.15416	3.09	0.042	0.3221	0.0089	0.1126	0.0051
MC30_45	52.57624	1.9626	0.1101	0.0064	-0.039017	3.871	0.083	0.407	0.0091	0.0238	0.0024
MC30_46	58.30904	1.972	0.0559	0.0028	0.38225	3.08	0.039	0.3161	0.0073	0.00613	0.00084
MC30_47	51.67959	2.5907	0.136	0.019	-0.59321	5.66	0.085	0.564	0.018	0.0452	0.0091
MC30_48	53.50455	2.4047	0.087	0.017	-0.32552	6.83	0.13	0.723	0.024	0.028	0.011
MC30_49	53.19149	3.1123	0.111	0.034	-0.81451	6.692	0.091	0.469	0.015	0.047	0.034
MC30_50	35.97122	6.0815	0.233	0.059	-0.7853	5.009	0.088	0.4146	0.0097	0.24	0.13
MC30_51	58.99705	1.6359	0.0595	0.0025	0.44412	3.534	0.038	0.3439	0.007	0.00499	0.00078
MC30_52	58.03831	1.92	0.072	0.014	-0.36481	4.553	0.091	0.408	0.017	0.013	0.0056
MC30_53	58.65103	1.6512	0.0612	0.0026	0.021797	3.418	0.035	0.3548	0.0078	0.0066	0.00087
					averages:	U (ppm)		Th (ppm)		Pb (ppm)	
						3.788422		0.5335		0.02784533	

Appendix C: Additional Maps of the Magnet Cove Igneous Complex

Plate 1: Detailed geologic map of the MCIC from Erickson and Blade (1963).